MITSUBISHI ELECTRIC RESEARCH LABORATORIES
https://www.merl.com

Diversity Gain Analysis of Distributed CDD Systems in Non-identical Fading Channels

Kim, Kyeong Jin; Liu, Hongwu; Ding, Zhiguo; Orlik, Philip V.; Poor, H. Vincent

TR2021-024 April 04, 2021

Abstract

This paper investigates the diversity gain of a distributed cyclic delay diversity (dCDD) scheme for cyclic-prefixed single carrier systems in non-identical fading channels. Nonidentical small-scale fading is assumed in the environment, in which non-identical line-of-sight and non-line-of-sight fading coexist. A condition for dCDD resulting in intersymbol interference free reception at the receiver, has been extended to this new channel environment. For an overpopulated system setup, a generalized performance analysis, which has not been available from existing works, has been conducted after developing closed-form expressions for the distribution of the signal-to-noise ratio (SNR) realized at the receiver. Since the order statistics are involved in the statistical properties of the SNR, the corresponding spacing statistics are utilized to derive feasible closed-form expressions. The finalized closed-form expressions are shown to provide very reliable outage probability and spectral efficiency of dCDD for underpopulated and overpopulated systems. An asymptotic performance analysis verifies the maximum achievable diversity of the dCDD even in the overpopulated case within the considered channel environment. Link-level simulations are conducted and these verify the maximum achievable diversity gain.

IEEE Transactions on Communications

Mitsubishi Electric Research Laboratories, Inc.
201 Broadway, Cambridge, Massachusetts 02139

Diversity Gain Analysis of Distributed CDD Systems in Non-identical Fading Channels

Kyeong Jin Kim, *Senior Member, IEEE,*, Hongwu Liu, *Senior Member, IEEE,*, Zhiguo Ding, *Fellow, IEEE*, Philip V. Orlik, *Senior Member, IEEE,*, and H. Vincent Poor, *Life Fellow, IEEE*

***Abstract*—This paper investigates the diversity gain of a distributed cyclic delay diversity (dCDD) scheme for cyclic-prefixed single carrier systems in non-identical fading channels. Non-identical small-scale fading is assumed in the environment, in which non-identical line-of-sight and non-line-of-sight fading coexist. A condition for dCDD resulting in intersymbol interference free reception at the receiver, has been extended to this new channel environment. For an overpopulated system setup, a generalized performance analysis, which has not been available from existing works, has been conducted after developing closed-form expressions for the distribution of the signal-to-noise ratio (SNR) realized at the receiver. Since the order statistics are involved in the statistical properties of the SNR, the corresponding spacing statistics are utilized to derive feasible closed-form expressions. The finalized closed-form expressions are shown to provide very reliable outage probability and spectral efficiency of dCDD for underpopulated and overpopulated systems. An asymptotic performance analysis verifies the maximum achievable diversity of the dCDD even in the overpopulated case within the considered channel environment. Link-level simulations are conducted and these verify the maximum achievable diversity gain.**

***Index Terms*—Distributed single carrier system, cyclic delay diversity, diversity gain, non-identical frequency selective fading, coexisting line-of-sight and non-line-of-sight paths.**

I. Introduction

The increasing proliferation of massive wireless devices and tremendous multimedia traffic lead to stringent requirements on 5G-and-beyond wireless communication systems. Massive connectivity, energy efficiency, and low latency transmissions are deemed as key performance metrics for evaluating wireless techniques in emerging applications such as autonomous vehicles, intelligent factories, and tactile internet [2]–[6]. As a promising diversity technique for wireless communications, transmit diversity has gained considerable attention. For example, orthogonal transmit diversity, space-time spreading, phase-switched transmit diversity, and delay diversity are well known techniques for achieving transmit diversity [7], [8]. Considering the diversity deterioration resulting from the absence of multi-path propagation and limited space for multi-antenna deployments, distributed transmission strategies have been proposed to achieve geographically enabled transmit diversity, including distributed space-time coding [9], [10], distributed maximal ratio transmission (dMRT) [11], [12], and distributed relaying [13]. It is also the case that a full rate orthogonal space-time block code is not known for a general number of distributed transmitters. In contrast to the conventional maximal ratio transmission scheme proposed by [14] and [15], dMRT can achieve diversity gain for a general number of single antenna transmitters by increasing the receive signal-to-noise ratio (SNR) over independent frequency selective fading channels. However, exact knowledge of channel state information at the transmitter (CSIT) is required, which is a challenging problem in a distributed communications system.

To achieve transmit diversity gain, cyclic delay diversity (CDD) has been widely used in practical Orthogonal Frequency Division Multiplexing (OFDM)-based wireless systems such as [16], [17], and [18] since it does not require CSIT. Although CDD requires lower complexity, in general, forward error correction is also required for OFDM transmissions to convert spatial diversity into frequency diversity [19]. Also, conventional CDD-based communications systems apply CDD among antennas that are installed at the same transmitter [17]–[21]. In contrast to such conventional CDD, distributed CDD (dCDD) that distributes CDD among single antenna equipped transmitters has been developed using different schemes. For example, the authors of [22] developed a multi-relay selection scheme to apply dCDD among the selected relays for cooperative relaying communications. Additionally, the authors of [23] integrated a selective random CDD scheme with joint cooperative relaying and hybrid automatic repeat request for two-hop vehicular communications.

Cyclic-prefixed single carrier (CP-SC) transmission has been also proposed for several wireless systems [24] considering more practical issues such as peak-to-average ratio, power-backing off, and dynamic range of the linear amplifier [25]. Several works [19]–[22] that exploit these benefits have attempted to use CDD among antennas. The recent work [26] proposed dCDD for CP-SC transmissions. Since then, CP-SC based dCDD has been applied to different types of wireless system such as spectrum sharing systems [27], [28], physical layer secrecy systems [29], [30], and cooperative transmit diversity systems [31]. For frequency selective fading channels, it has been shown in [32] and [33] that multipath diversity can be achieved without utilizing channel equalization [20]. Multiuser diversity can also be exploited to achieve the maximum diversity by using either the best terminal selection [32]

Kyeong Jin Kim and Philip V. Orlik are with Mitsubishi Electric Research Laboratories (MERL), Cambridge, MA 02139 USA (e-mail: kkim@merl.com; porlik@merl.com).

Hongwu Liu is with Shandong Jiaotong University, Jinan 250357, China (e-mail: hong.w.liu@hotmail.com).

Zhiguo Ding is with the School of Electrical and Electronic Engineering, The University of Manchester, Manchester M13 9PL, U.K. (e-mail: zhiguo.ding@manchester.ac.uk).

H. Vincent Poor is with the Department of Electrical Engineering, Princeton University, Princeton, NJ 08544 USA (e-mail: poor@princeton.edu).

Parts of this paper were presented at the 2018 IEEE International Conference on Communications [1].

or best relay selection [33]. In contrast to the approaches of [22] and [23], recent approaches [27]–[31] can jointly exploit multipath diversity and multiuser diversity among distributed transmitters and in frequency selective fading channels. Thus, it is expected that the dCDD scheme employed by [27]–[31] will lead to distributed systems with greater throughput. Although there are several works [34]–[36] that derive the probability density function (PDF) of the partial sum of the order statistics, they mainly assume either identical Rayleigh fading or identical frequency selective fading channels, so that it is not straightforward to use them in diversity gain analysis. Thus, to the best our knowledge, the diversity gain analysis of dCDD for a general scenario has never been investigated for non-identical frequency selective channels.

In this paper, we address the following three issues.

- Except [26], others systems [27], [29], [30] assume an underpopulated system, in which the total number of remote radio units (RRUs) is less than the total number of RRUs that is supported by dCDD, due to a limited coverage of the feasible analysis.
- The analysis provided by [26] works only for less than three RRUs in the independent but non-identically distributed (i.n.i.d.) frequency selective fading environment. It is a more realistic system setup that a plurality of RRUs exist above what dCDD can support. In addition, as an RRU can be recognized as one of the antennas of the distributed antenna system (DAS), the distances from RRUs to the receiver (RX) will be distributed in the DAS. Thus, it is an open problem how to analyze performance of dCDD in the overpopulated distributed system in environments with i.n.i.d. frequency selective fading channels.
- Due to a widespread installation of RRUs, line-of-sight (LoS) and none-line-of-sight (nLoS) paths may coexist in the target environments. Thus, it is also necessary to investigate the impact of coexisting LoS and nLoS paths on the performance.

Considering these three issues, we summarize the following three contributions in this paper.

- Motivated by the work conducted in [26], we derive a new received signal model. The distribution of the SNR realized at the RX is derived based on the order statistics [37] and the spacing statistics [38]. Since reliability of the partial fraction (PF)-based derivation tends to decline as either the maximum number of multipath components over the whole system or the maximum allowed number of RRUs increases, we use a very reliable approximation in its final step. Thus, in contrast to the derivation used in [26], a new derivation can support more than three RRUs even for an overpopulated system.
- Based on the derived distributions, we separately derive closed-form expressions for the outage probability and spectral efficiency.
- From the asymptotic outage probability in the high SNR region, the achievable diversity gain is derived. For various system settings and channel parameters, their impacts on the diversity gain are investigated. In addition, the impact of a different ratio of the LoS path to the nLoS path on the diversity gain is analyzed. Link-level simulation results verify the derived maximum diversity gain.

Notation: $\boldsymbol{I}_N$ is an $N \times N$ identity matrix; $\mathbf{0}$ denotes an all zeros matrix of appropriate dimensions; $\mathcal{N}\left(\mu, \sigma^2\right)$ denotes the complex Gaussian distribution with mean μ and variance σ^2; $\mathbb{B}$ denotes the set composed of 0 and 1; $\mathbb{N}_0$ denotes the set of non-negative integers; and $\mathbb{C}$ denotes the set of complex numbers, so that $\mathbb{C}^{m\times n}$ denotes the vector space of all $m \times n$ complex matrices. $F_{\varphi}(\cdot)$ denotes the cumulative distribution function (CDF) of the random variable (RV) φ, whereas its PDF is denoted by $f_{\varphi}(\cdot)$; and the binomial coefficient is denoted by $\binom{n}{k} \triangleq \frac{n!}{(n-k)!k!}$. For a vector $\boldsymbol{a}$, $\mathfrak{N}(\boldsymbol{a})$ denotes the cardinality of $\boldsymbol{a}$; and $\boldsymbol{a}(l)$ denotes its lth element. For a vector $\boldsymbol{a}_{i,|N|}$ with the second subscript defining its cardinality, $\mathrm{sum}(\boldsymbol{a}_{i,|N|}) = c$ denotes the sum for all sets of positive indices of $[\boldsymbol{a}_i(1), \ldots, \boldsymbol{a}_i(N)]$ satisfying $\sum_{j=1}^{N} \boldsymbol{a}_i(j) = c$. When the second parameter of the binomial coefficient notation is represented by a vector, $\boldsymbol{a}_{i,|N|}$, the binomial coefficient notation becomes the multinomial coefficient as follows: $\binom{c}{\boldsymbol{a}_{i,|N|}} \triangleq \frac{c!}{\boldsymbol{a}_i(1)!\ldots\boldsymbol{a}_i(N)!}$.

For a set of continuous random variables, $\{x_1, x_2, \ldots, x_N\}$, $x_{\langle i \rangle}$ denotes the ith smallest random variable, so that it becomes the ith order statistic with $0 < x_{\langle 1 \rangle} \leq x_{\langle 2 \rangle} \leq \ldots \leq x_{\langle N \rangle} < \infty$. By defining the differences between two adjacent order statistics, that is, $y_i \triangleq x_{\langle i \rangle} - x_{\langle i-1 \rangle}$ for $i \geq 2$ and $y_1 = x_{\langle 1 \rangle}$, y_is become independent [39] with $y_i \geq 0$, $\forall i$, and form the spacing statistics. Each of the elements of the order statistics can be expressed in terms of the spacing statistics as follows: $x_{\langle i \rangle} = \sum_{j=1}^{i} y_j$. The Jacobian matrix for this transformation is lower triangular with ones on the diagonal, so that its determinant is one.

II. System and Channel Models

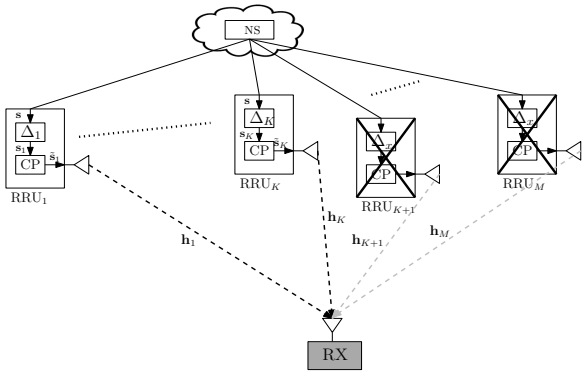

Fig. 1. Illustration of the proposed dCDD-based distributed single carrier system.

A block diagram of a proposed cooperative CP-SC system is provided in Fig. 1. The network server (NS) provides backhaul communications to M RRUs via very reliable backhaul. For practical deployment constraint, only one single antenna is assumed at the RRUs and RX. Due to the maximum available

number of RRUs, K, which is supported by dCDD, Fig. 1 shows that the first K RRUs are working as dCDD RRUs, whereas the remaining $M-K$ crossed-out RRUs are in the idle state, a state that the RRU is not allowed to transmit signals by the NS. With the aid of Global Navigation Satellite System or 802.11-based precision time protocol [40], [41], the RRUs are assumed to be clock synchronized to the NS. Thus, the NS works as the clock master as well. Phase synchronization is also assumed among the NS and RRUs. Although RRUs are geographically distributed with respect to the NS, we assume that the NS, M RRUs, and RX are co-located, so that the RX can receive the signals simultaneously from K RRUs by the control of the NS.

A. Channel model

With the deployment in the multipath-rich environments, we assume that a wireless channel from the mth RRU to RX, denoted by $\boldsymbol{h}_m$, is assumed to be distributed by frequency selective fading. In addition, due to geographically distributed RRUs with respect to the RX, we assume the following things:

- Due do different distances from the RRUs to RX, small-scale fading and large-scale fading are not identical in the whole system.
- Channels are uncorrelated with one another.
- LoS path and nLoS path are co-existing in the environment [27]. A similar model is also employed for the ultra dense cloud small cell network [42]. A binary Bernoulli process is used to model a random selection of LoS and nLoS paths [27]. Due to distributed distances in the considered system, the selection probability of LoS and nLoS paths are not identical.

Under these assumptions, a wireless channel $\boldsymbol{h}_m$, from the mth RRU to RX, is expressed as follows [27]:

$$\begin{aligned}\boldsymbol{h}_m &= \mathbb{I}_{m,\mathrm{L}}(d_m)^{-\epsilon_{\mathrm{L}}/2}\tilde{\boldsymbol{h}}_{m,\mathrm{L}} + \mathbb{I}_{m,\mathrm{nL}}(d_m)^{-\epsilon_{\mathrm{nL}}/2}\tilde{\boldsymbol{h}}_{m,\mathrm{nL}} \\ &= \mathbb{I}_{m,\mathrm{L}}\sqrt{\alpha_{m,\mathrm{L}}}\tilde{\boldsymbol{h}}_{m,\mathrm{L}} + \mathbb{I}_{m,\mathrm{nL}}\sqrt{\alpha_{m,\mathrm{nL}}}\tilde{\boldsymbol{h}}_{m,\mathrm{nL}} \end{aligned} \quad (1)$$

where small-scale frequency selective fading channels [17], [24] are respectively denoted by $\tilde{\boldsymbol{h}}_{m,\mathrm{L}}$ and $\tilde{\boldsymbol{h}}_{m,\mathrm{nL}}$ for LoS and nLoS paths with $\mathfrak{N}(\tilde{\boldsymbol{h}}_{m,\mathrm{L}}) = N_{m,\mathrm{L}}$ and $\mathfrak{N}(\tilde{\boldsymbol{h}}_{m,\mathrm{nL}}) = N_{m,\mathrm{nL}}$, whose elements are assumed to be i.i.d. according to $\mathcal{CN}(0,1)$. In addition, $\alpha_{m,\mathrm{L}} \triangleq (d_m)^{-\epsilon_{\mathrm{L}}}$ and $\alpha_{m,\mathrm{nL}} \triangleq (d_m)^{-\epsilon_{\mathrm{nL}}}$, that is, a distance dependent path loss model is used to model a large scale fading. Since RRUs are geographically distributed in the considered system, different path losses can be assumed as well. The euclidean distance from the mth RRU to RX is denoted by d_m. Path-loss exponents of the LoS path and nLoS path are respectively defined by ϵ_{L} and ϵ_{nL}. In addition, $\mathbb{I}_{m,\mathrm{L}}$ is a Bernoulli variable with probability $P_r(\mathbb{I}_{m,\mathrm{L}} = 1) = \mathcal{G}_{m,\mathrm{L}}$ and $P_r(\mathbb{I}_{m,\mathrm{L}} = 0) = 1 - \mathcal{G}_{m,\mathrm{L}}$. Similarly, $\mathbb{I}_{m,\mathrm{nL}} \triangleq 1 - \mathbb{I}_{m,\mathrm{L}}$ is a complementary Bernoulli variable of $\mathbb{I}_{m,\mathrm{L}}$ with $P_r(\mathbb{I}_{m,\mathrm{nL}} = 1) = \mathcal{G}_{m,\mathrm{nL}} \triangleq 1 - \mathcal{G}_{m,\mathrm{L}}$. Again, due to geographically distributed RRUs with respect to the RX, $\tilde{\boldsymbol{h}}_{m,\mathrm{L}}$ and $\tilde{\boldsymbol{h}}_{m,\mathrm{nL}}$ are composed by different numbers of multipath components.

B. Summary of dCDD operation

Since dCDD is proposed for CP-SC transmissions, the NS prepares a block symbol $\boldsymbol{s} \in \mathbb{C}^{Q\times 1}$, composed of Q modulated symbols, for transmissions. Thus, Q is a system parameter that is determined by the NS.

1) Information for frequency selective channels: Since we assume an overpopulated system, the number of RRUs, M, in the distributed system is above the maximum number of RRUs, K, that supports dCDD without causing inter-symbol interference (ISI) at the RX. To select K RRUs out of M RRUs, the NS requires an additional information, being fed back by the RX[1]. One of the unique features of dCDD is that the RX needs to feed back only $N_{\max}$[2], which is defined by $N_{\max} \triangleq \max(N_{m,\mathrm{L}}, N_{m,\mathrm{nL}}, \forall m)$. Note that this parameter is determined from frequency selective fading channels.

*2) Information for channel quality indicator (*CQI*):* In addition, the NS needs to use a CQI to select K RRUs for dCDD operation. This CQI should be prepared from channel estimates. With a very reliable channel estimate, $\hat{\boldsymbol{h}}_m$, at the RX, we can have $\hat{\boldsymbol{h}}_m \approx \boldsymbol{h}_m,\ \forall m$. Thus, the RX can compute mth CQI as follows:

$$\mathrm{CQI}_m \triangleq \mathbb{I}_{m,\mathrm{L}}\alpha_{m,\mathrm{L}}\|\tilde{\boldsymbol{h}}_{m,\mathrm{L}}\|^2 + \mathbb{I}_{m,\mathrm{nL}}\alpha_{m,\mathrm{nL}}\|\tilde{\boldsymbol{h}}_{m,\mathrm{nL}}\|^2 \quad (2)$$

and then arrange them by their magnitudes in such a way that $\mathrm{CQI}_{\langle 1\rangle} \le \mathrm{CQI}_{\langle 2\rangle} \le \ldots \le \mathrm{CQI}_{\langle M\rangle}$. Note that a pilot block symbol, $\boldsymbol{s}_p \in \mathbb{C}^{Q\times 1}$ that satisfies $E\{\boldsymbol{s}_p\} = \boldsymbol{0}$ and $E\{\boldsymbol{s}_p(\boldsymbol{s}_p)^H\} = \boldsymbol{I}_Q$, is used for CP-SC transmissions at the RRUs. After receiving the pilot symbol in the training period, the RX measures its channel strength. Now to specify the order statistics for CQIs, the RX sends a list indexing CQI, i.e., $\mathbb{X} \triangleq (\langle 1\rangle, \langle 2\rangle, \ldots, \langle M\rangle)$, from the least to greatest, to the NS. Only sending this list to the NS, feedback overhead can be reduced.

3) Number of dCDD RRUs: Now using available Q, $N_{\max}$, and $\mathbb{X}$, the NS selects K RRUs, where K is determined by $K = \lfloor \frac{Q}{N_{\max}} \rfloor$ with $\lfloor\cdot\rfloor$ denoting the floor function, to provide greater aggregated channel quality at the RX[3]. This can be possible by selecting K RRUs indexed by the last K elements of $\mathbb{X}$. Un-selected RRUs for dCDD will be in the idle state, a state that the NS does not allow them to transmit the signals to the RX. By applying these procedures, an ISI-free reception can be possible at the RX even for simultaneous CP-SC transmissions. It is worthwhile to note that dCDD does not require full CSIT. Instead, it requires Q, $N_{\max}$, and $\mathbb{X}$, the last two of which need to be fed back by the RX. In general, $N_{\max}$ is usually specified by $N_{\max} = Q/4$ [24], [25] in wireless systems, so that four RRUs can be supported as dCDD RRUs.

[1]When the system assumes a single tap channel such as [22], [23], then the RX dose not need to feedback any information.

[2]$N_{\max}$ can be fed back to the transmitter in the form of CQI or precoding type indicator as those in Physical Uplink Control Channel or Physical Uplink Shared Channel of Long Term Evolution [43].

[3]This number is different from that of [22], [23] that assume one tap channel. Thus, this is more effective in covering non-identical frequency selective fading channels.

4) CDD delay assignment: Now using $N_{\max}$ and K, the NS assigns CDD delay to each of the dCDD RRUs according to

$$\Delta_m = (m-1)N_{\max}, \text{ for } 1 \le m \le K. \tag{3}$$

Applying the CDD delay at each CDD-RRU is equal to multiply the input symbol block $\boldsymbol{s}$ by the permutation matrix $\boldsymbol{P}_m \in \mathbb{B}^{Q\times Q}$, which is a circularly shifted identity matrix of size Q, $\boldsymbol{I}_Q$. It is clear that $\boldsymbol{P}_m$ is a right circulant matrix of order Q. An amount of its circular shifting down is determined by Δ_m. Thus, each dCDD RRU requires only simple mathematical operation. In order to verify ISI-free operation achieved by the CDD delay assignment, we provide one example as follows:

5) Example 1: Let us assume that $Q=6$, $M=2$, $N_{\langle 1\rangle,\mathrm{L}}=2$, and $N_{\langle 2\rangle,\mathrm{L}}=3$. Then, we can have $N_{\max}=3$ and $K=2$. Thus, for $\mathcal{G}_{1,\mathrm{L}}=\mathcal{G}_{2,\mathrm{L}}=1$, $\tilde{\boldsymbol{H}}_{\langle 1\rangle,\mathrm{L}}$ is given by (4) provided at the top of the next page. In (4), we have defined $\Delta_0=0$ and $\Delta_1=3$. Similarly, for $\Delta_0=2$ and $\Delta_1=5$, $\tilde{\boldsymbol{H}}_{\langle 1\rangle,\mathrm{L}}$ is given by (5) at the top of the next page that applies a random CDD assignment [23]. From (4) and (5), non-overlapped channel elements are observed in each of the components of $\tilde{\boldsymbol{H}}_{\langle 1\rangle,\mathrm{L}}$. Thus, ISI-free CP-SC transmissions can be achieved when K is determined by $K=\lfloor \frac{Q}{N_{\max}} \rfloor$.

6) Received signal at the RX: According to dCDD, the RX can receive the ISI-free signals from K dCDD RRUs simultaneously. To simplify notation, we use $\langle m\rangle \triangleq \langle M-K+m\rangle$ in the sequel. Thus, the received signal, $\boldsymbol{r}\in\mathbb{C}^{Q\times 1}$, at the RX is given by

$$\begin{aligned}\boldsymbol{r} = \sum\nolimits_{m=1}^{K} \Big(&\mathbb{I}_{\langle m\rangle,\mathrm{L}} \sqrt{P_T \alpha_{\langle m\rangle,\mathrm{L}}}\, \tilde{\boldsymbol{H}}_{\langle m\rangle,\mathrm{L}} \boldsymbol{P}_m + \\ &\mathbb{I}_{\langle m\rangle,\mathrm{nL}} \sqrt{P_T \alpha_{\langle m\rangle,\mathrm{nL}}}\, \tilde{\boldsymbol{H}}_{\langle m\rangle,\mathrm{nL}} \boldsymbol{P}_m \Big) \boldsymbol{s} + \boldsymbol{z}\end{aligned} \tag{6}$$

where P_T denotes the transmission power at the dCDD RRUs. Equivalent channel matrices $\tilde{\boldsymbol{H}}_{\langle m\rangle,\mathrm{L}} \in \mathbb{C}^{Q\times Q}$ and $\tilde{\boldsymbol{H}}_{\langle m\rangle,\mathrm{nL}} \in \mathbb{C}^{Q\times Q}$ are right circulant matrices, mainly determined by $\tilde{\boldsymbol{h}}_{\langle m\rangle,\mathrm{L}} \in \mathbb{C}^{N_{m,\mathrm{L}}\times 1}$, $\tilde{\boldsymbol{h}}_{\langle m\rangle,\mathrm{nL}} \in \mathbb{C}^{N_{m,\mathrm{nL}}\times 1}$, and additional zeros. According to [33], $\tilde{\boldsymbol{H}}_{\langle m\rangle,\mathrm{L}}$ and $\tilde{\boldsymbol{H}}_{\langle m\rangle,\mathrm{nL}}$ are precisely determined as follows:

$$\begin{aligned}\tilde{\boldsymbol{H}}_{\langle m\rangle,\mathrm{L}} &= \boldsymbol{W}^H \boldsymbol{\Lambda}_{\langle m\rangle,\mathrm{L}} \boldsymbol{W} \text{ and} \\ \tilde{\boldsymbol{H}}_{\langle m\rangle,\mathrm{nL}} &= \boldsymbol{W}^H \boldsymbol{\Lambda}_{\langle m\rangle,\mathrm{nL}} \boldsymbol{W}\end{aligned} \tag{7}$$

where $\boldsymbol{W} \in \mathbb{C}^{Q\times Q}$ is the discrete Fourier matrix with its conjugate transposition denoted by $\boldsymbol{W}^H$. In addition, $\boldsymbol{\Lambda}_{\langle m\rangle,\mathrm{L}} \in \mathbb{C}^{Q\times Q}$ and $\boldsymbol{\Lambda}_{\langle m\rangle,\mathrm{nL}} \in \mathbb{C}^{Q\times Q}$ are diagonal matrices with the qth diagonal elements respectively determined by

$$\begin{aligned}\lambda_{q,\mathrm{L}} &= \sum\nolimits_{l=1}^{N_{\langle m\rangle,\mathrm{L}}} \tilde{\boldsymbol{h}}_{\langle m\rangle,\mathrm{L}}(l) e^{-j2\pi q(l-1)/Q} \text{ and} \\ \lambda_{q,\mathrm{nL}} &= \sum\nolimits_{l=1}^{N_{\langle m\rangle,\mathrm{nL}}} \tilde{\boldsymbol{h}}_{\langle m\rangle,\mathrm{nL}}(l) e^{-j2\pi q(l-1)/Q}.\end{aligned} \tag{8}$$

An additive noise is modeled by $\boldsymbol{z} \sim \mathcal{N}(\boldsymbol{0}, \sigma_z^2 \boldsymbol{I}_Q)$. For a transmission block symbol, $\boldsymbol{s}$, we also assume that $E\{\boldsymbol{s}\}=\boldsymbol{0}$ and $E\{\boldsymbol{s}\boldsymbol{s}^H\}=\boldsymbol{I}_Q$. Note that in the representation of (6), the order statistics are involved in the channel related terms and indicator functions, $\mathbb{I}_{\langle m\rangle,\mathrm{L}}$ and $\mathbb{I}_{\langle m\rangle,\mathrm{nL}}$.

III. Performance analysis

By using independent Bernoulli RVs and uncorrelated channels, the SNR realized at the RX is given by

$$\begin{aligned}\gamma \triangleq \sum\nolimits_{m=1}^{K} \big(&\mathbb{I}_{\langle m\rangle,\mathrm{L}} \tilde{\alpha}_{\langle m\rangle,\mathrm{L}} \|\tilde{\boldsymbol{h}}_{\langle m\rangle,\mathrm{L}}\|^2 + \\ &\mathbb{I}_{\langle m\rangle,\mathrm{nL}} \tilde{\alpha}_{\langle m\rangle,\mathrm{nL}} \|\tilde{\boldsymbol{h}}_{\langle m\rangle,\mathrm{nL}}\|^2 \big) = \sum\nolimits_{m=1}^{K} \gamma_{\langle m\rangle}\end{aligned} \tag{9}$$

where $\tilde{\alpha}_{\langle m\rangle,\mathrm{L}} = \rho\alpha_{\langle m\rangle,\mathrm{L}}$, $\tilde{\alpha}_{\langle m\rangle,\mathrm{nL}} = \rho\alpha_{\langle m\rangle,\mathrm{nL}}$ with $\rho \triangleq P_T/\sigma_z^2$, and $\gamma_{\langle m\rangle} \triangleq \big(\mathbb{I}_{\langle m\rangle,\mathrm{L}} \tilde{\alpha}_{\langle m\rangle,\mathrm{L}} \|\tilde{\boldsymbol{h}}_{\langle m\rangle,\mathrm{L}}\|^2 + \mathbb{I}_{\langle m\rangle,\mathrm{nL}} \tilde{\alpha}_{\langle m\rangle,\mathrm{nL}} \|\tilde{\boldsymbol{h}}_{\langle m\rangle,\mathrm{nL}}\|^2\big)$. Note that ISI-free reception at the RX makes an aggregated SNR at the RX, so that improved performance can be achieved.

Corollary 1: Due to randomly coexisting LoS and nLoS paths, the CDF of $\gamma_{\langle m\rangle}$ is given by

$$\begin{aligned}F_{\gamma_{\langle m\rangle}}(x) = &\mathcal{G}_{\langle m\rangle,\mathrm{L}} F_{\tilde{\alpha}_{\langle m\rangle,\mathrm{L}} \|\tilde{\boldsymbol{h}}_{\langle m\rangle,\mathrm{L}}\|^2}(x) + \\ &\mathcal{G}_{\langle m\rangle,\mathrm{nL}} F_{\tilde{\alpha}_{\langle m\rangle,\mathrm{nL}} \|\tilde{\boldsymbol{h}}_{\langle m\rangle,\mathrm{nL}}\|^2}(x)\end{aligned} \tag{10}$$

where $F_{\tilde{\alpha}_{\langle m\rangle,\mathrm{L}} \|\tilde{\boldsymbol{h}}_{\langle m\rangle,\mathrm{L}}\|^2}(x)$ and $F_{\tilde{\alpha}_{\langle m\rangle,\mathrm{nL}} \|\tilde{\boldsymbol{h}}_{\langle m\rangle,\mathrm{nL}}\|^2}(x)$ are respectively CDFs of $\tilde{\alpha}_{\langle m\rangle,\mathrm{L}} \|\tilde{\boldsymbol{h}}_{\langle m\rangle,\mathrm{L}}\|^2$ and $\tilde{\alpha}_{\langle m\rangle,\mathrm{nL}} \|\tilde{\boldsymbol{h}}_{\langle m\rangle,\mathrm{nL}}\|^2$.

Proof: The CDF of γ_m is given by

$$\begin{aligned}F_{\gamma_{\langle m\rangle}}(x) = &Pr(\gamma_{\langle m\rangle} < x | \mathbb{I}_{\langle m\rangle,\mathrm{L}}) Pr(\mathbb{I}_{\langle m\rangle,\mathrm{L}}) + \\ &Pr(\gamma_{\langle m\rangle} < x | \mathbb{I}_{\langle m\rangle,\mathrm{nL}}) Pr(\mathbb{I}_{\langle m\rangle,\mathrm{nL}})\end{aligned} \tag{11}$$

so that we can derive (10). ■

Due to employed channel assumptions, CDFs of $\tilde{\alpha}_{\langle m\rangle,\mathrm{L}} \|\tilde{\boldsymbol{h}}_{\langle m\rangle,\mathrm{L}}\|^2$ and $\tilde{\alpha}_{\langle m\rangle,\mathrm{nL}} \|\tilde{\boldsymbol{h}}_{\langle m\rangle,\mathrm{nL}}\|^2$ are respectively expressed as follows [12]:

$$\begin{aligned}F_{\tilde{\alpha}_{\langle m\rangle,\mathrm{L}} \|\tilde{\boldsymbol{h}}_{\langle m\rangle,\mathrm{L}}\|^2}(x) &= \frac{\gamma_l(N_{\langle m\rangle,\mathrm{L}}, x/\tilde{\alpha}_{\langle m\rangle,\mathrm{L}})}{\Gamma(N_{\langle m\rangle,\mathrm{L}})} \text{ and} \\ F_{\tilde{\alpha}_{\langle m\rangle,\mathrm{nL}} \|\tilde{\boldsymbol{h}}_{\langle m\rangle,\mathrm{nL}}\|^2}(x) &= \frac{\gamma_l(N_{\langle m\rangle,\mathrm{nL}}, x/\tilde{\alpha}_{\langle m\rangle,\mathrm{nL}})}{\Gamma(N_{\langle m\rangle,\mathrm{nL}})}\end{aligned} \tag{12}$$

where $\Gamma(\cdot)$ and $\gamma_l(\cdot,\cdot)$ respectively denote the complete gamma function and incomplete lower-gamma function. Now using (12), (10) can be evaluated in the following corollary.

Corollary 2: The CDF and PDF of $\gamma_{\langle m\rangle}$ are evaluated as follows:

$$\begin{aligned}F_{\gamma_{\langle m\rangle}}(x) &= \sum\nolimits_{p_m=0}^{1} \sum\nolimits_{r_m=0}^{p_m} (\mathcal{G}_{\langle m\rangle,\mathrm{L}})^{p_m-r_m} (\mathcal{G}_{\langle m\rangle,\mathrm{nL}})^{r_m} \\ &\qquad \Psi_{\langle m\rangle} e^{-\tilde{a}_{\langle m\rangle} x} x^{\langle \tilde{m}\rangle} \\ &= \mathbb{X}_{\langle m\rangle} e^{-\tilde{a}_{\langle m\rangle} x} x^{\langle \tilde{m}\rangle} \text{ and} \\ f_{\gamma_{\langle m\rangle}}(x) &= \mathbb{Y}_{\langle m\rangle} e^{-\breve{a}_{\langle m\rangle} x} x^{\langle \breve{m}\rangle - 1}\end{aligned} \tag{13}$$

where $\tilde{a}_{\langle m\rangle} \triangleq (q_m - r_m)/\tilde{\alpha}_{\langle m\rangle,\mathrm{L}} + r_m/\tilde{\alpha}_{\langle m\rangle,\mathrm{nL}}$ and $\tilde{m} \triangleq (\boldsymbol{t}_{m,|N_{\langle m\rangle,\mathrm{L}}|})^T \boldsymbol{l}_{m,|N_{\langle m\rangle,\mathrm{L}}|} + (\boldsymbol{t}_{m,|N_{\langle m\rangle,\mathrm{nL}}|})^T \boldsymbol{k}_{m,N_{\langle m\rangle,\mathrm{nL}}}$ for $\boldsymbol{t}_{m,|N_{\langle m\rangle,\mathrm{L}}|} \triangleq [0,1,\ldots,N_{\langle m\rangle,\mathrm{L}}-1]^T$, $\boldsymbol{t}_{m,|N_{\langle m\rangle,\mathrm{nL}}|} \triangleq [0,1,\ldots,N_{\langle m\rangle,\mathrm{nL}}-1]^T$, $\boldsymbol{l}_{m,N_{\langle m\rangle,\mathrm{L}}}$, and $\boldsymbol{k}_{m,N_{\langle m\rangle,\mathrm{nL}}}$, which are respectively satisfying $\mathrm{sum}(\boldsymbol{l}_{m,|N_{\langle m\rangle,\mathrm{L}}|}) = p_m - r_m$ and $\mathrm{sum}(\boldsymbol{k}_{m,|N_{\langle m\rangle,\mathrm{nL}}|}) = r_m$. Note that $\boldsymbol{l}_{m,N_{\langle m\rangle,\mathrm{L}}} \in \mathbb{N}_0^{|N_{\langle m\rangle,\mathrm{L}}|}$ and $\boldsymbol{k}_{m,N_{\langle m\rangle,\mathrm{nL}}} \in \mathbb{N}_0^{|N_{\langle m\rangle,\mathrm{nL}}|}$ are related with the multinomial theorem. Furthermore, we have defined $\Psi_{\langle m\rangle}$ provided at the top of the next page and $\mathbb{X}_{\langle m\rangle} \triangleq \sum_{p_m=0}^{1} \sum_{r_m=0}^{p_m} (\mathcal{G}_{\langle m\rangle,\mathrm{L}})^{1-r_m} (\mathcal{G}_{\langle m\rangle,\mathrm{nL}})^{r_m} \Psi_{\langle m\rangle}$. In

$$\tilde{\boldsymbol{H}}_{\langle 1\rangle,L}=\begin{bmatrix} \tilde{\boldsymbol{h}}_{\langle 1\rangle,\mathrm{L}}(1) & \tilde{\boldsymbol{h}}_{\langle 2\rangle,\mathrm{L}}(3) & \tilde{\boldsymbol{h}}_{\langle 2\rangle,\mathrm{L}}(2) & \tilde{\boldsymbol{h}}_{\langle 2\rangle,\mathrm{L}}(1) & 0 & \tilde{\boldsymbol{h}}_{\langle 1\rangle,\mathrm{L}}(2) \\ \tilde{\boldsymbol{h}}_{\langle 1\rangle,\mathrm{L}}(2) & \tilde{\boldsymbol{h}}_{\langle 1\rangle,\mathrm{L}}(1) & \tilde{\boldsymbol{h}}_{\langle 2\rangle,\mathrm{L}}(3) & \tilde{\boldsymbol{h}}_{\langle 2\rangle,\mathrm{L}}(2) & \tilde{\boldsymbol{h}}_{\langle 2\rangle,\mathrm{L}}(1) & 0 \\ 0 & \tilde{\boldsymbol{h}}_{\langle 1\rangle,\mathrm{L}}(2) & \tilde{\boldsymbol{h}}_{\langle 1\rangle,\mathrm{L}}(1) & \tilde{\boldsymbol{h}}_{\langle 2\rangle,\mathrm{L}}(3) & \tilde{\boldsymbol{h}}_{\langle 2\rangle,\mathrm{L}}(2) & \tilde{\boldsymbol{h}}_{\langle 2\rangle,\mathrm{L}}(1) \\ \tilde{\boldsymbol{h}}_{\langle 2\rangle,\mathrm{L}}(1) & 0 & \tilde{\boldsymbol{h}}_{\langle 1\rangle,\mathrm{L}}(2) & \tilde{\boldsymbol{h}}_{\langle 1\rangle,\mathrm{L}}(1) & \tilde{\boldsymbol{h}}_{\langle 2\rangle,\mathrm{L}}(3) & \tilde{\boldsymbol{h}}_{\langle 2\rangle,\mathrm{L}}(2) \\ \tilde{\boldsymbol{h}}_{\langle 2\rangle,\mathrm{L}}(2) & \tilde{\boldsymbol{h}}_{\langle 2\rangle,\mathrm{L}}(1) & 0 & \tilde{\boldsymbol{h}}_{\langle 1\rangle,\mathrm{L}}(2) & \tilde{\boldsymbol{h}}_{\langle 1\rangle,\mathrm{L}}(1) & \tilde{\boldsymbol{h}}_{\langle 2\rangle,\mathrm{L}}(3) \\ \tilde{\boldsymbol{h}}_{\langle 2\rangle,\mathrm{L}}(3) & \tilde{\boldsymbol{h}}_{\langle 2\rangle,\mathrm{L}}(2) & \tilde{\boldsymbol{h}}_{\langle 2\rangle,\mathrm{L}}(1) & 0 & \tilde{\boldsymbol{h}}_{\langle 1\rangle,\mathrm{L}}(2) & \tilde{\boldsymbol{h}}_{\langle 1\rangle,\mathrm{L}}(1) \end{bmatrix}. \tag{4}$$

$$\tilde{\boldsymbol{H}}_{\langle 1\rangle,\mathrm{L}}=\begin{bmatrix} \tilde{\boldsymbol{h}}_{\langle 2\rangle,\mathrm{L}}(2) & \tilde{\boldsymbol{h}}_{\langle 2\rangle,\mathrm{L}}(1) & 0 & \tilde{\boldsymbol{h}}_{\langle 1\rangle,\mathrm{L}}(2) & \tilde{\boldsymbol{h}}_{\langle 1\rangle,\mathrm{L}}(1) & \tilde{\boldsymbol{h}}_{\langle 2\rangle,\mathrm{L}}(3) \\ \tilde{\boldsymbol{h}}_{\langle 2\rangle,\mathrm{L}}(3) & \tilde{\boldsymbol{h}}_{\langle 2\rangle,\mathrm{L}}(2) & \tilde{\boldsymbol{h}}_{\langle 2\rangle,\mathrm{L}}(1) & 0 & \tilde{\boldsymbol{h}}_{\langle 1\rangle,\mathrm{L}}(2) & \tilde{\boldsymbol{h}}_{\langle 1\rangle,\mathrm{L}}(1) \\ \tilde{\boldsymbol{h}}_{\langle 1\rangle,\mathrm{L}}(1) & \tilde{\boldsymbol{h}}_{\langle 2\rangle,\mathrm{L}}(3) & \tilde{\boldsymbol{h}}_{\langle 2\rangle,\mathrm{L}}(2) & \tilde{\boldsymbol{h}}_{\langle 2\rangle,\mathrm{L}}(1) & 0 & \tilde{\boldsymbol{h}}_{\langle 1\rangle,\mathrm{L}}(2) \\ \tilde{\boldsymbol{h}}_{\langle 1\rangle,\mathrm{L}}(2) & \tilde{\boldsymbol{h}}_{\langle 1\rangle,\mathrm{L}}(1) & \tilde{\boldsymbol{h}}_{\langle 2\rangle,\mathrm{L}}(3) & \tilde{\boldsymbol{h}}_{\langle 2\rangle,\mathrm{L}}(2) & \tilde{\boldsymbol{h}}_{\langle 2\rangle,\mathrm{L}}(1) & 0 \\ 0 & \tilde{\boldsymbol{h}}_{\langle 1\rangle,\mathrm{L}}(2) & \tilde{\boldsymbol{h}}_{\langle 1\rangle,\mathrm{L}}(1) & \tilde{\boldsymbol{h}}_{\langle 2\rangle,\mathrm{L}}(3) & \tilde{\boldsymbol{h}}_{\langle 2\rangle,\mathrm{L}}(2) & \tilde{\boldsymbol{h}}_{\langle 2\rangle,\mathrm{L}}(1) \\ \tilde{\boldsymbol{h}}_{\langle 2\rangle,\mathrm{L}}(1) & 0 & \tilde{\boldsymbol{h}}_{\langle 1\rangle,\mathrm{L}}(2) & \tilde{\boldsymbol{h}}_{\langle 1\rangle,\mathrm{L}}(1) & \tilde{\boldsymbol{h}}_{\langle 2\rangle,\mathrm{L}}(3) & \tilde{\boldsymbol{h}}_{\langle 2\rangle,\mathrm{L}}(2) \end{bmatrix}. \tag{5}$$

$$\Psi_{\langle m\rangle}\triangleq\sum\nolimits_{\mathrm{sum}(\boldsymbol{l}_{m,|N_{\langle m\rangle,\mathrm{L}}|})=p_m-r_m}\left[\binom{p_m-r_m}{\boldsymbol{l}_{m,|N_{\langle m\rangle,\mathrm{L}}|}}\prod\nolimits_{t_m=0}^{N_{\langle m\rangle,\mathrm{L}}-1}(1/t_m!)^{l_{m,t_m+1}}\right]\sum\nolimits_{\mathrm{sum}(\boldsymbol{k}_{m,|N_{\langle m\rangle,\mathrm{nL}}|})=r_m}\left[\binom{r_m}{\boldsymbol{k}_{m,|N_{\langle m\rangle,\mathrm{nL}}|}}\prod\nolimits_{t_m=0}^{N_{\langle m\rangle,\mathrm{nL}}-1}(1/t_m!)^{k_{m,t_m+1}}\right]$$

addition, $\mathbb{Y}_{\langle m\rangle}\triangleq\sum_{r_m=0}^{1}\left(\frac{\mathcal{G}_{\langle m\rangle,\mathrm{L}}}{\Gamma(N_{\langle m\rangle,\mathrm{L}})(\tilde{\alpha}_{\langle m\rangle,\mathrm{L}})^{N_{\langle m\rangle,\mathrm{L}}}}\right)^{1-r_m}\left(\frac{\mathcal{G}_{\langle m\rangle,\mathrm{nL}}}{\Gamma(N_{\langle m\rangle,\mathrm{nL}})(\tilde{\alpha}_{\langle m\rangle,\mathrm{nL}})^{N_{\langle m\rangle,\mathrm{nL}}}}\right)^{r_m}$, $\breve{a}_{\langle m\rangle}\triangleq(1-r_m)/\tilde{\alpha}_{\langle m\rangle,\mathrm{L}}+r_m/\tilde{\alpha}_{\langle m\rangle,\mathrm{nL}}$, and $\breve{m}\triangleq N_{\langle m\rangle,\mathrm{L}}+r_m(1-N_{\langle m\rangle,\mathrm{L}})+r_m(N_{\langle m\rangle,\mathrm{nL}}-1)$.

Proof: By using binomial and multinomial theorems [44, Eq. (1.111)], we can readily derive (13). ∎

Due to different distances from the dCDD RRUs to RX, $X_m\triangleq\gamma_{\langle m\rangle}$ has a different distribution depending on its index m. In addition, dCDD makes the SNR, γ, aggregate K largest SNRs when there is no ISI reception at the RX. Thus, it is necessary to use the order statistics in analyzing the statistical properties of the SNR.

For the order statistics, $\{\gamma_{\langle m\rangle}, m=1,\ldots,K\}$, the joint PDF of $X_1,\ldots,X_K$ is given by [37]

$$f_{X_1,\ldots,X_K}(x_1,x_2,\ldots,x_K)=\mathrm{Per}\boldsymbol{A}_K \tag{14}$$

where

$$\boldsymbol{A}_K\triangleq\frac{1}{(M-K)!}\begin{bmatrix} F_1(x_1) & f_1(x_1) & \ldots & f_1(x_K) \\ F_2(x_1) & f_2(x_1) & \ldots & f_2(x_K) \\ \vdots & \vdots & \ldots & \vdots \\ F_M(x_1) & f_M(x_1) & \ldots & f_M(x_K) \\ \underbrace{M-K} & \underbrace{1} & \underbrace{1} & \underbrace{1} \end{bmatrix} \tag{15}$$

with $F_j(\cdot)$ and $f_j(\cdot)$ respectively denoting the CDF and PDF of γ_j, the SNR. Their expressions are similarly defined as those of (13). Also, we define $\left[\underbrace{\boldsymbol{a}_1}_{i}\ \underbrace{\boldsymbol{a}_2}_{j}\right]$ denoting i copies of the first column vector $\boldsymbol{a}_1$ and j copies of the second column vector $\boldsymbol{a}_2$, and so on. The permanent of the square matrix $\boldsymbol{A}$, denoted by $\mathrm{Per}\boldsymbol{A}$, is defined similar to the definition of the matrix determinant except that all signs are taken to be positive [37]. For example, for a square matrix $\boldsymbol{A}$, given by $\boldsymbol{A}=\begin{bmatrix} a & b \\ c & d \\ \underbrace{1} & \underbrace{1} \end{bmatrix}$, we have $\mathrm{Per}\boldsymbol{A}=ad+bc$.

With some manipulations, a desired compact expression for $\mathrm{Per}\boldsymbol{A}_K$ is given by

$$\mathrm{Per}\boldsymbol{A}_K=\sum\nolimits_{\substack{n_1,\ldots,n_K \\ n_1\neq n_2\neq\ldots\neq n_K}}\prod\nolimits_{i=1}^{K}\mathbb{Y}_{n_i}e^{-\breve{a}_{n_i}x_i}(x_i)^{\breve{m}_{n_i}-1}\prod\nolimits_{i=K+1}^{M}(\mathbb{X}_{n_i}e^{-\tilde{a}_{n_i}x_i}(x_1)^{\tilde{m}_{n_i}}) \tag{16}$$

where $\sum_{\substack{n_1,\ldots,n_K \\ n_1\neq n_2\neq\ldots\neq n_K}}\triangleq\sum_{n_1=1}^{K}\sum_{\substack{n_2=1 \\ n_2\neq n_1}}^{K}\cdots\sum_{\substack{n_K=1 \\ n_K\neq n_1 \\ \ldots \\ n_K\neq n_{K-1}}}^{M}$.

Based on $\mathrm{Per}\boldsymbol{A}_K$, the moment geometric function (MGF) for γ is provided in the following theorem.

Theorem 1: The MGF of the SNR realized at the RX by dCDD is given by

$$M_\gamma(s)=\widetilde{\sum}_{\substack{n_1,\ldots,n_K \\ n_1\neq n_2\neq\ldots\neq n_K}}\prod\nolimits_{m=1}^{K}(K+1-m)^{-e_m}\Gamma(e_m)\left[\prod\nolimits_{m=1}^{K}(s+q_m)^{-e_m}\right] \tag{17}$$

where $\widetilde{\sum}_{\substack{n_1,\ldots,n_K \\ n_1\neq n_2\neq\ldots\neq n_K}}\triangleq\sum_{\substack{n_1,\ldots,n_K \\ n_1\neq n_2\neq\ldots\neq n_K}}\mathbb{C}_{M,K}\sum_{\mathrm{sum}(\boldsymbol{a}_{2,|2|})=\breve{m}_2-1}\binom{\breve{m}_2-1}{\boldsymbol{a}_{2,|2|}}\ldots\sum_{\mathrm{sum}(\boldsymbol{a}_{K,|K|})=\breve{m}_K-1}\binom{\breve{m}_K-1}{\boldsymbol{a}_{K,|K|}}$ with $\{\boldsymbol{a}_{j,|j|}\in\mathbb{N}_0^{|j|},\forall j\}$, $\mathbb{C}_{M,K}\triangleq(\prod_{i=1}^{K}\mathbb{Y}_{n_i})(\prod_{i=K+1}^{M}\mathbb{X}_i)$, $e_1\triangleq\breve{m}_1+\sum_{j=2}^{K}\boldsymbol{a}_{j,|j|}(1)+\sum_{i=K+1}^{M}\tilde{m}_i$, $e_{k\geq 2}\triangleq\sum_{j=2}^{K}\boldsymbol{a}_{j,|j|}(m)+1$, $q_1\triangleq\frac{1}{K}(\sum_{j=1}^{K}\breve{a}_j+\sum_{i=K+1}^{M}\tilde{a}_i)$, and $q_{k\geq 2}\triangleq\frac{1}{K+1-m}\left(\sum_{j=m}^{K}\breve{a}_j\right)$, with $\breve{a}_i\triangleq\breve{a}_{n_i}$, $\breve{m}_i\triangleq\breve{m}_{n_i}$, and $\tilde{a}_{n_i}\triangleq\tilde{a}_i$.

Proof: See Appendix A. ∎

Due to geometrically distributed RRUs, it is given that $q_i \neq q_j,\ \forall i \neq j$. Thus, the number of repeated poles of the MGF is determined by K, the maximum number of RRUs for dCDD. However, as either M, K, or $N_{\max}$ increases, the PF makes the computation of the inverse MGF (IMGF) easy to diverge, so that it is necessary to develop a more reliable expression for the MGF.

Corollary 3: According to [45], a very reliable and approximated expression for $\prod_{m=1}^{K}(s+q_m)^{-e_m}$, a part of the MGF, $M_\gamma(s)$, is given by

$$\prod_{m=1}^{K}(s+q_m)^{-e_m} = \sum_{l=0}^{N_1}\delta_l(b_I)^{-l}(1/b_I+s)^{-F_d-l} \quad (18)$$

where N_1 denotes an upper limit summation. In addition, $F_d \overset{\triangle}{=} \sum_{m=1}^{K} e_m$, $b_I \overset{\triangle}{=} \min(1/q_1,\ldots,1/q_K)$, and $\delta_l \overset{\triangle}{=} \frac{1}{l}\sum_{i=1}^{l} i r_i \delta_{l-i}$ with $\delta_0 = 1$ and $r_i = \sum_{m=1}^{K}\frac{e_m}{i}(1-b_I q_m)^i$.

Proof: See Appendix B. ∎

It was verified by [45] that when $\max_i \left|\frac{(1-b_I q_i)}{(1+b_I s)}\right| < 1,\ \forall s$, (18) is a valid approximation. *Corollary 3* provides the MGF expressed by the weighted sum of N_1+1 terms, each of which is proportional to $(1/b_I+s)^{-F_d-l}$. Since the IMGF of $(1/b_I+s)^{-F_d-l}$ is $\frac{1}{\Gamma(F_d+l)}e^{-x/b_I}x^{F_d+l-1}$, the following corollary can be immediately derived.

Corollary 4: The PDF and CDF of γ can be expressed by a finite number of gamma distributions. Its expression is given by

$$f_\gamma(x) = \widetilde{\sum_{\substack{n_1,\ldots,n_K \\ n_1\neq n_2\neq\ldots\neq n_K}}} \prod_{m=1}^{K}(K+1-m)^{-e_m}\Gamma(e_m) \sum_{l=0}^{N_1}\delta_l(b_I)^{-l}\frac{1}{\Gamma(F_d+l)}e^{-x/b_I}x^{F_d+l-1} \text{ and}$$

$$F_\gamma(x) = \widetilde{\sum_{\substack{n_1,\ldots,n_K \\ n_1\neq n_2\neq\ldots\neq n_K}}} \prod_{m=1}^{K}(K+1-m)^{-e_m}\Gamma(e_m) \sum_{l=0}^{N_1}\delta_l(b_I)^{-l}\frac{(b_I)^{F_d+l}}{\Gamma(F_d+l)}\gamma_l(F_d+l, x/b_I). \quad (19)$$

Corollary 5: Only when two RRUs are selected for dCDD operation, which is the best case of [26] on the number of RRUs for performance analysis, the PDF and CDF of γ are respectively given by

$$f_\gamma(x) = \widetilde{\sum_{\substack{n_1,n_2 \\ n_1\neq n_2}}} \prod_{m=1}^{2}(3-m)^{-e_m}\Gamma(e_m) \sum_{l=0}^{N_1}\delta_l(b_I)^{-l}\frac{1}{\Gamma(F_d+l)}e^{-x/b_I}x^{F_d+l-1} \text{ and}$$

$$F_\gamma(x) = \widetilde{\sum_{\substack{n_1,n_2 \\ n_1\neq n_2}}} \prod_{m=1}^{2}(3-m)^{-e_m}\Gamma(e_m) \sum_{l=0}^{N_1}\delta_l(b_I)^{-l}\frac{(b_I)^{F_d+l}}{\Gamma(F_d+l)}\gamma_l(F_d+l, x/b_I) \quad (20)$$

where the re-used notations in (20) can be easily inferred from the derivation of (19).

Note that N_1 controls the accuracy of the distributions in representing them with a finite number of gamma distributions. In addition, F_d is a key parameter that determines an asymptotic performance in the high SNR region. Based on (19), performance metrics, such as the outage probability and spectral efficiency will be derived next.

A. Performance metrics

1) Outage probability: Since a closed-form expression for the CDF of the SNR realized at the RX is available, the outage probability (OP) at the outage threshold, o_{th}, is given by

$$\text{OP} = \widetilde{\sum_{\substack{n_1,\ldots,n_K \\ n_1\neq n_2\neq\ldots\neq n_K}}} \prod_{m=1}^{K}(K+1-m)^{-e_m}\Gamma(e_m) \sum_{l=0}^{N_1}\delta_l(b_I)^{-l}\frac{(b_I)^{F_d+l}}{\Gamma(F_d+l)}\gamma_l(F_d+l, o_{\text{th}}/b_I). \quad (21)$$

2) Spectral efficiency: The spectral efficiency (SE) can be derived as follows:

$$\begin{aligned}\text{SE} &= \int_0^\infty \log_2(1+x)f_\gamma(x)dx \\ &= \frac{1}{\ln(2)}\widetilde{\sum_{\substack{n_1,\ldots,n_K \\ n_1\neq n_2\neq\ldots\neq n_K}}} \prod_{m=1}^{K}(K+1-m)^{-e_m}\Gamma(e_m) \sum_{l=0}^{N_1}\frac{\delta_l(b_I)^{-l}}{\Gamma(F_d+l)}\int_0^\infty \log(1+x)e^{-x/b_I}x^{F_d+l-1}dx. \quad (22)\end{aligned}$$

After representing $\log(1+x)$ is terms of Meijer G-function [46], and applying [47, eq. (07.34.22.0003.01)], (22) can be evaluated as follows:

$$\text{SE} = \frac{1}{\ln(2)}\widetilde{\sum_{\substack{n_1,\ldots,n_K \\ n_1\neq n_2\neq\ldots\neq n_K}}} \prod_{m=1}^{K}(K+1-m)^{-e_m}\Gamma(e_m) \sum_{l=0}^{N_1}\frac{\delta_l(b_I)^{F_d}}{\Gamma(F_d+l)}G_{3,2}^{1,3}\big(b_I\big|\begin{matrix}1-F_d-l, 1, 1\\ 1, 0\end{matrix}\big) \quad (23)$$

where $G_{p,q}^{m,n}\big(t\big|\begin{matrix}a_1,\ldots,a_n,a_{n+1},\ldots,a_p\\ b_1,\ldots,b_m,b_{m+1},\ldots,b_q\end{matrix}\big)$ denotes the Meijer G-function [44, Eq. (9.301)].

To find insightful meaning from the derivations, we conduct performance analysis in the high SNR region next.

B. Asymptotic performance analysis

In the high SNR region, (12) can be approximated as

$$F_{\tilde{\alpha}_{\langle m\rangle,\text{L}}\|\tilde{\boldsymbol{h}}_{\langle m\rangle,\text{L}}\|^2}(x) \approx \frac{\rho^{-N_{\langle m\rangle,\text{L}}}x^{N_{\langle m\rangle,\text{L}}}}{\Gamma(N_{\langle m\rangle,\text{L}}+1)(\alpha_{\langle m\rangle,\text{L}})^{N_{\langle m\rangle,\text{L}}}} \text{ and}$$

$$F_{\tilde{\alpha}_{\langle m\rangle,\text{nL}}\|\tilde{\boldsymbol{h}}_{\langle m\rangle,\text{nL}}\|^2}(x) \approx \frac{\rho^{-N_{\langle m\rangle,\text{nL}}}x^{N_{\langle m\rangle,\text{nL}}}}{\Gamma(N_{\langle m\rangle,\text{nL}}+1)(\alpha_{\langle m\rangle,\text{nL}})^{N_{\langle m\rangle,\text{nL}}}}. \quad (24)$$

Thus, the corresponding expression for the CDF of $\gamma_{\langle m\rangle}$ can be derived as follows:

$$F_{\gamma_{\langle m\rangle}}(x) \approx \mathbb{F}_{\langle m\rangle}\rho^{-N_{\langle m\rangle}}x^{N_{\langle m\rangle}} \quad (25)$$

where

$$N_{\langle m\rangle} = \begin{cases} N_{\langle m\rangle,\text{L}}, & \text{for } N_{\langle m\rangle,\text{L}} \leq N_{\langle m\rangle,\text{nL}}, \\ N_{\langle m\rangle,\text{nL}}, & \text{for } N_{\langle m\rangle,\text{L}} > N_{\langle m\rangle,\text{nL}} \end{cases} \quad (26)$$

and $\mathbb{F}_{\langle m\rangle}$ provided at the top of the next page. Similarly, the PDF of $\gamma_{\langle m\rangle}$ in the high SNR region can be expressed as follows:

$$f_{\gamma_{\langle m\rangle}}(x) \approx \mathbb{P}_{\langle m\rangle}\rho^{-N_{\langle m\rangle}}e^{-x/(\rho\mathbb{B}_{\langle m\rangle})}x^{N_{\langle m\rangle}-1} \quad (27)$$

$$\mathbb{F}_{\langle m\rangle}=\begin{cases}\mathcal{G}_{\langle m\rangle,\mathrm{L}}\frac{(\alpha_{\langle m\rangle,\mathrm{L}})^{-N_{\langle m\rangle,\mathrm{L}}}}{\Gamma(N_{\langle m\rangle,\mathrm{L}}+1)}, & \text{for } N_{\langle m\rangle,\mathrm{L}}<N_{\langle m\rangle,\mathrm{nL}},\\ \mathcal{G}_{\langle m\rangle,\mathrm{nL}}\frac{(\alpha_{\langle m\rangle,\mathrm{nL}})^{-N_{\langle m\rangle,\mathrm{nL}}}}{\Gamma(N_{\langle m\rangle,\mathrm{nL}}+1)}, & \text{for } N_{\langle m\rangle,\mathrm{L}}>N_{\langle m\rangle,\mathrm{nL}},\\ \mathcal{G}_{\langle m\rangle,\mathrm{L}}\frac{(\alpha_{\langle m\rangle,\mathrm{L}})^{-N_{\langle m\rangle,\mathrm{L}}}}{\Gamma(N_{\langle m\rangle,\mathrm{L}}+1)}+\mathcal{G}_{\langle m\rangle,\mathrm{nL}}\frac{(\alpha_{\langle m\rangle,\mathrm{nL}})^{-N_{\langle m\rangle,\mathrm{nL}}}}{\Gamma(N_{\langle m\rangle,\mathrm{nL}}+1)}, & \text{for } N_{\langle m\rangle,\mathrm{L}}=N_{\langle m\rangle,\mathrm{nL}}.\end{cases}$$

where

$$\mathbb{B}_{\langle m\rangle}=\begin{cases}\alpha_{\langle m\rangle,\mathrm{L}}, & \text{for } N_{\langle m\rangle,\mathrm{L}}<N_{\langle m\rangle,\mathrm{nL}},\\ \alpha_{\langle m\rangle,\mathrm{nL}}, & \text{for } N_{\langle m\rangle,\mathrm{L}}>N_{\langle m\rangle,\mathrm{nL}},\\ \alpha_{\langle m\rangle,\mathrm{L}}+\alpha_{\langle m\rangle,\mathrm{nL}}, & \text{for } N_{\langle m\rangle,\mathrm{L}}=N_{\langle m\rangle,\mathrm{nL}}, \text{ and}\end{cases} \quad (28)$$

and $\mathbb{P}_{\langle m\rangle}$ defined at the top of the next page. Note that, in the high SNR region, we approximate the CDF and PDF of $\gamma_{\langle m\rangle}$ in terms of $\min(N_{\langle m\rangle,\mathrm{L}},N_{\langle m\rangle,\mathrm{nL}})$. Based on (25) and (27), $\mathrm{Per}\boldsymbol{A}_K^{\mathrm{as}}$ can be given by

$$\mathrm{Per}\boldsymbol{A}_K^{\mathrm{as}}=\sum\nolimits_{\substack{n_1,\ldots,n_K\\ n_1\neq n_2\neq\ldots\neq n_K}}\mathbb{D}_{M,K}e^{-x_1/(\rho\mathbb{B}_{\langle n_1\rangle})} x_1^{(N_{\langle n_1\rangle}+\sum_{i=K+1}^{M}N_{\langle n_i\rangle}-1)}\big(\prod\nolimits_{i=2}^{K}e^{-x_i/(\rho\mathbb{B}_{\langle n_i\rangle})}(x_i)^{N_{\langle n_i\rangle}-1}\big)\rho^{-G_d} \quad (29)$$

where $\mathbb{D}_{M,K}\overset{\triangle}{=}\big(\prod_{i=K+1}^{M}\mathbb{F}_{\langle n_i\rangle}\big)\big(\prod_{i=1}^{K}\mathbb{P}_{\langle n_i\rangle}\big)$, and $G_d=\sum_{i=1}^{M}N_{\langle n_i\rangle}$. Applying the spacing statistics again to x_is, (29) can be computed as (30) provided at the top of the next page. Note that (30) shows that $\mathrm{Per}\boldsymbol{A}_K^{\mathrm{as}}$ is expressed in the form of a product of functions, each of which is a function of only one of the y_is. Since y_is are independent of one another, the MGF can be derived as follows:

$$M_\gamma^{\mathrm{as}}(s)=\widetilde{\sum}_{\substack{n_1,\ldots,n_K\\ n_1\neq n_2\neq\ldots\neq n_K}}\Big(\prod\nolimits_{m=1}^{K}(K+1-m)^{-e_m^{\mathrm{as}}}\Gamma(e_m^{\mathrm{as}})\Big)(s+q_1^{\mathrm{as}})^{-e_1^{\mathrm{as}}}\prod\nolimits_{k=2}^{K}(s+q_k^{\mathrm{as}})^{-e_k^{\mathrm{as}}}\rho^{-G_d} \quad (31)$$

where $\widetilde{\sum}_{\substack{n_1,\ldots,n_K\\ n_1\neq n_2\neq\ldots\neq n_K}}\overset{\triangle}{=}\sum_{\substack{n_1,\ldots,n_K\\ n_1\neq n_2\neq\ldots\neq n_K}}\mathbb{D}_{M,K}\sum_{\mathrm{sum}(\boldsymbol{w}_{2,|2|})=N_{\langle n_2\rangle}-1}\binom{N_{\langle n_2\rangle}-1}{\boldsymbol{w}_{2,|2|}}\sum_{\mathrm{sum}(\boldsymbol{w}_{3,|3|})=N_{\langle n_3\rangle}-1}\binom{N_{\langle n_3\rangle}-1}{\boldsymbol{w}_{3,|3|}}\ldots\sum_{\mathrm{sum}(\boldsymbol{w}_{K,|K|})=N_{\langle n_K\rangle}-1}\binom{N_{\langle n_K\rangle}-1}{\boldsymbol{w}_{K,|K|}}$, $q_1^{\mathrm{as}}\overset{\triangle}{=}\frac{1}{K}\sum_{j=1}^{K}\frac{1}{\rho\mathbb{B}_{\langle n_j\rangle}}$, $q_{k\geq 2}^{\mathrm{as}}\overset{\triangle}{=}\frac{1}{K+1-k}\sum_{j=k}^{K}\frac{1}{\rho\mathbb{B}_{\langle n_j\rangle}}$, $e_1^{\mathrm{as}}\overset{\triangle}{=}N_{\langle n_1\rangle}+\sum_{j=2}^{K}\boldsymbol{w}_{j,|j|}(1)+\sum_{i=K+1}^{M}N_{\langle n_i\rangle}$, and $e_{k\geq 2}^{\mathrm{as}}\overset{\triangle}{=}\sum_{j=k}^{K}\boldsymbol{w}_{j,|j|}(k)+1$. Thus, we can see that $q_i\neq q_j$ for $i\neq j$ due to a different number of summations and normalizing constants.

Theorem 2: The dCDD can achieve the asymptotic diversity gain, $G_d=\sum_{i=1}^{M}N_{\langle n_i\rangle}$, over non-identical frequency selective fading channels.

Proof: It is necessary to study the asymptotic behavior of $M_\gamma(s)$ as $\rho\to\infty$, which shows that $M_\gamma(s)\overset{\rho\to\infty}{\approx}\widetilde{\sum}_{\substack{n_1,\ldots,n_K\\ n_1\neq n_2\neq\ldots\neq n_K}}\big(\prod_{m=1}^{K}(K+1-m)^{-e_m^{\mathrm{as}}}\Gamma(e_m^{\mathrm{as}})\big)s^{-\sum_{k=1}^{K}e_k^{\mathrm{as}}}\rho^{-G_d}$. Since $1+\sum_{l=1}^{|j|}\boldsymbol{w}_{j,|j|}(l)=N_{\langle n_j\rangle}$, we can have $\sum_{k=1}^{K}e_k^{\mathrm{as}}=G_d$. Thus, $M_\gamma(s)\overset{\rho\to\infty}{\approx}\widetilde{\sum}_{\substack{n_1,\ldots,n_K\\ n_1\neq n_2\neq\ldots\neq n_K}}\big(\prod_{m=1}^{K}(K+1-m)^{-e_m^{\mathrm{as}}}\Gamma(e_m^{\mathrm{as}})\big)s^{-G_d}\rho^{-G_d}$, which verifies the asymptotic diversity gain G_d. ∎

From this asymptotic MGF, the asymptotic CDF of γ can be derived as

$$F_\gamma^{\mathrm{as}}(x)\overset{\rho\to\infty}{\approx}\widetilde{\sum}_{\substack{n_1,\ldots,n_K\\ n_1\neq n_2\neq\ldots\neq n_K}}\Big(\prod\nolimits_{m=1}^{K}(K+1-m)^{-e_m^{\mathrm{as}}}\Gamma(e_m^{\mathrm{as}})\Big)\frac{1}{\Gamma(G_d+1)}\Big(\frac{\rho}{x}\Big)^{-G_d} \quad (32)$$

so that, at a given outage threshold, o_{th}, we can have $\mathrm{OP}^{\mathrm{as}}\propto(\frac{\rho}{\mathrm{o}_{th}})^{-G_d}$.

Theorem 2 can be rephrased in the following Corollaries.

Corollary 6: For non-identical frequency selective fading channels, dCDD can achieve the maximum diversity gain, G_d, irrespective of how many RRUs are selected as the dCDD RRUs. That is, the diversity gain is independent of K.

Proof: From the expression for $G_d=\sum_{m=1}^{M}N_{\langle n_m\rangle}=\sum_{m=1}^{M}\min(N_{m,\mathrm{L}},N_{m,\mathrm{nL}})$, we can see that the minimum number of multipath components of the frequency selective channel connected to each of M RRUs contributes to the diversity gain. Since dCDD makes the RX aggregate K SNRs including the greatest SNR, realized by M RRUs, the achievable diversity gain depends on M, the total number of RRUs in the system. When $K=1$, the dCDD-based system will be similar to the cooperative systems [32] and [33] that achieve the same diversity gain by employing best relay selection. ∎

Corollary 7: For non-identical frequency selective fading channels, dCDD provides a greater diversity gain as the total number of RRUs increases. That is, the diversity gain depends on M as the summation of multipath components.

Proof: From the expression for G_d, we can see that G_d increases as the number of RRUs increases depending on the type of the frequency selective fading channels in LoS dominant, nLoS dominant, and coexisting LoS and nLoS environments. When the environment is LoS dominant, the diversity gain is given by $G_d=\sum_{m=1}^{M}N_{m,\mathrm{L}}$. Refer to the derivations from [26], [32], and [33]. ∎

IV. Simulation Results

As an additional notation, $\prec a,b,c,d\succ$ denotes that the first element, a, is assigned to RRU_1, whereas the forth element, d, is assigned to RRU_4. In the link-level simulations, we assume the following common parameters:

- Quadrature phase-shift keying (QPSK) modulation is used with $P_T=1$.
- The transmission block size for CP-SC transmissions is $Q=32$.
- Path-loss exponents are respectively assumed to be $\epsilon_{\mathrm{L}}=2.09$ and $\epsilon_{\mathrm{nL}}=3.75$ for LoS and nLoS paths [48].

$$\mathbb{P}_{\langle m\rangle} = \begin{cases} \mathcal{G}_{\langle m\rangle,\mathrm{L}} \frac{(\alpha_{\langle m\rangle,\mathrm{L}})^{-N_{\langle m\rangle,\mathrm{L}}}}{\Gamma(N_{\langle m\rangle,\mathrm{L}})} \triangleq P_{m,1}, & \text{for } N_{\langle m\rangle,\mathrm{L}} < N_{\langle m\rangle,\mathrm{nL}} \\ \mathcal{G}_{\langle m\rangle,\mathrm{nL}} \frac{(\alpha_{\langle m\rangle,\mathrm{nL}})^{-N_{\langle m\rangle,\mathrm{nL}}}}{\Gamma(N_{\langle m\rangle,\mathrm{nL}})} \triangleq P_{m,2}, & \text{for } N_{\langle m\rangle,\mathrm{L}} > N_{\langle m\rangle,\mathrm{nL}} \\ \sum_{l=0}^{1} (P_{m,1})^{1-l}(P_{m,2})^2, & \text{for } N_{\langle m\rangle,\mathrm{L}} = N_{\langle m\rangle,\mathrm{nL}}. \end{cases}$$

$$\begin{aligned} \mathrm{Per}\boldsymbol{A}_K^{\mathrm{as}} = \sum_{\substack{n_1,\ldots,n_K \\ n_1\neq n_2\neq\ldots\neq n_K}} \mathbb{D}_{M,K} \sum_{\mathrm{sum}(\boldsymbol{w}_{2,|2|})=N_{\langle n_2\rangle}-1} \binom{N_{\langle n_2\rangle}-1}{\boldsymbol{w}_{2,|2|}} \sum_{\mathrm{sum}(\boldsymbol{w}_{3,|3|})=N_{\langle n_3\rangle}-1} \binom{N_{\langle n_3\rangle}-1}{\boldsymbol{w}_{3,|3|}} \ldots \\ \sum_{\mathrm{sum}(\boldsymbol{w}_{K,|K|})=N_{\langle n_K\rangle}-1} \binom{N_{\langle n_K\rangle}-1}{\boldsymbol{w}_{K,|K|}} \Big[e^{-y_1/(\sum_{j=1}^{K}\rho\mathbb{B}_{\langle n_j\rangle})} y_1^{(N_{\langle n_1\rangle}+\sum_{j=2}^{K}\boldsymbol{w}_{j,|j|}(1)+\sum_{i=K+1}^{M}N_{\langle n_i\rangle}-1)} \Big] \\ \prod_{l=2}^{K} \big[e^{-y_l/(\sum_{j=l}^{K}\rho\mathbb{B}_{\langle n_j\rangle})} y_l^{(\sum_{j=l}^{K}\boldsymbol{w}_{j,|j|}(l))} \big] \rho^{-G_d}. \end{aligned} \tag{30}$$

- Locations of six RRUs are assumed to be $\prec (6.8 + j3.3), (4.4 + j2.5), (8.0 + j4.6), (9.0 + j1.7), (7.3 - j2.6), (10.3 - j0.5) \succ$. In addition, the RX is assumed to be placed at $(3.0 - j3.0)$.
- A fixed number is used for N_1 that controls the accuracy of the IMGF, i.e., $N_I = 100$.
- The SNR threshold causing an outage is given by $o_{\mathrm{th}} = 1$ dB.

To verify the performance metrics, we consider several scenarios as follows:

- $\mathbb{S}_1$: $M = 4$ with $N_{m,\mathrm{L}}s \prec 2, 3, 3, 2 \succ$ and $N_{m,\mathrm{nL}}s \prec 3, 2, 2, 4 \succ$.
- $\mathbb{S}_2$: $M = 5$ with $N_{m,\mathrm{L}}s \prec 3, 2, 2, 3, 3 \succ$ and $N_{m,\mathrm{nL}}s \prec 4, 3, 2, 2, 2 \succ$.
- $\mathbb{S}_3$: $M = 5$ with $N_{m,\mathrm{L}}s \prec 2, 3, 3, 2, 4 \succ$ and $N_{m,\mathrm{nL}}s \prec 3, 2, 2, 4, 3 \succ$.
- $\mathbb{S}_4$: $M = 5$ with $N_{m,\mathrm{L}}s \prec 3, 4, 4, 3, 5 \succ$ and $N_{m,\mathrm{nL}}s \prec 3, 2, 2, 4, 3 \succ$.
- $\mathbb{S}_5$: $M = 4$ with $N_{m,\mathrm{L}}s \prec 2, 3, 3, 2 \succ$ and $N_{m,\mathrm{nL}}s \prec 5, 4, 4, 6 \succ$.
- $\mathbb{S}_6$: $M = 4$ with $N_{m,\mathrm{L}}s \prec 3, 4, 4, 3 \succ$ and $N_{m,\mathrm{nL}}s \prec 3, 2, 2, 4 \succ$.
- $\mathbb{S}_7$: $M = 4$ with $N_{m,\mathrm{L}}s \prec 3, 4, 4, 3 \succ$ and $N_{m,\mathrm{nL}}s \prec 5, 4, 4, 6 \succ$.
- $\mathbb{S}_8$: $M = 4$ with $N_{m,\mathrm{L}}s \prec 4, 5, 5, 4 \succ$ and $N_{m,\mathrm{nL}}s \prec 3, 2, 2, 4 \succ$.
- $\mathbb{S}_9$: $M = 5$ with $N_{m,\mathrm{L}}s \prec 2, 3, 3, 2, 4 \succ$ and $N_{m,\mathrm{nL}}s \prec 5, 4, 4, 6, 1 \succ$.
- $\mathbb{S}_{10}$: $M = 6$ with $N_{m,\mathrm{L}}s \prec 2, 3, 3, 2, 4, 3 \succ$ and $N_{m,\mathrm{nL}}s \prec 5, 4, 4, 6, 1, 6 \succ$.

Note that $\mathcal{G}_{\mathrm{nL}}s$ can be obtained via $\mathcal{G}_{\mathrm{nL}}s = 1 - \mathcal{G}_{\mathrm{L}}s$. When $\mathcal{G}_{\mathrm{L}}s \prec 0.0, \ldots, 0.0 \succ$, this corresponds to the environment where only nLoS paths exist. In contrast, $\mathcal{G}_{\mathrm{L}}s \prec 1.0, \ldots, 1.0 \succ$ corresponds to the environment where only LoS paths exist. Note that $\mathbb{S}_1$, $\mathbb{S}_6$, and $\mathbb{S}_7$ specify various numbers of multipath components for small-scale fading channels respectively influenced by LoS and nLoS large-scale fading. The curves obtained by the link-level simulations are denoted by **Ex**. Analytically derived performance curves are denoted by **An**.

A. Performance analysis in terms of the OP

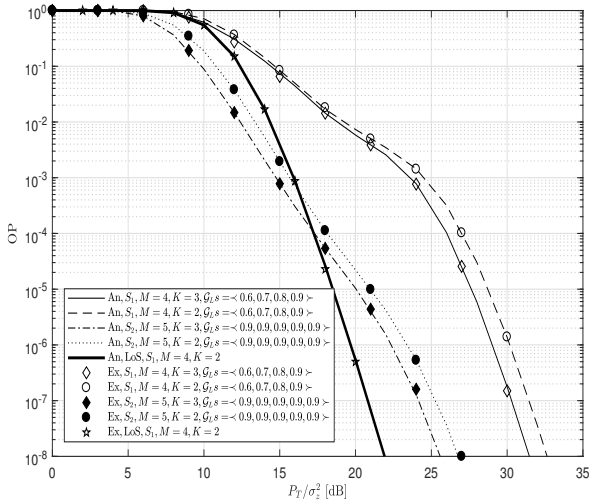

Fig. 2. OP for various scenarios.

1) Accuracy of the derivation: Fig. 2 shows the correctness of the analytically derived OP, which is given by (21), comparing with the corresponding exact OP. This figure also shows that as the more RRUs are involved in dCDD operation, K, at the same number of RRUs, M, a lower OP is obtained. We can also see that for the same number of dCDD RRUs, a more number of RRUs results in a lower OP. For general system parameters, M and K, the proposed derivations are seen to be very reliable and provide very accurate results. This figure also verifies the accuracy of the OP in the LoS-rich non-identical fading environment, which was mainly investigated by [26]. Thus, (21) can provide a reliable and approximation for the OP for various system and channel parameters.

2) Impact of selection probability of LoS path on the OP: To investigate the impact of selection probability of the LoS path, $\mathcal{G}_{\mathrm{L}}$, on the OP, we use scenario $\mathbb{S}_4$ with $K = 3$. Analytically derived OPs are obtained via (21). For this scenario, Fig. 3 shows the following observations:

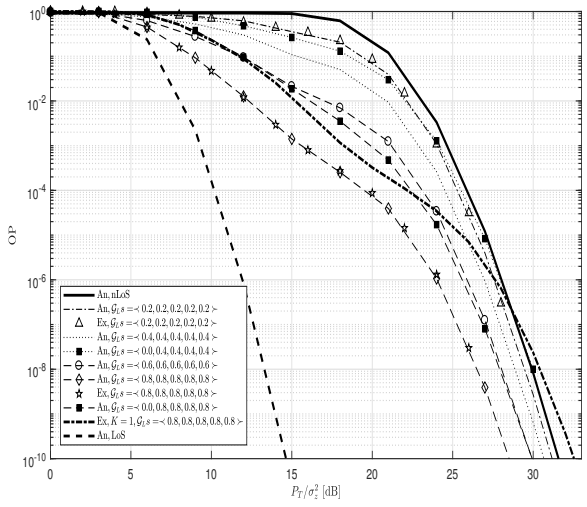

Fig. 3. Impact of $\mathcal{G}_L$ on the OP. Scenario $\mathbb{S}_4$ is used for this simulation.

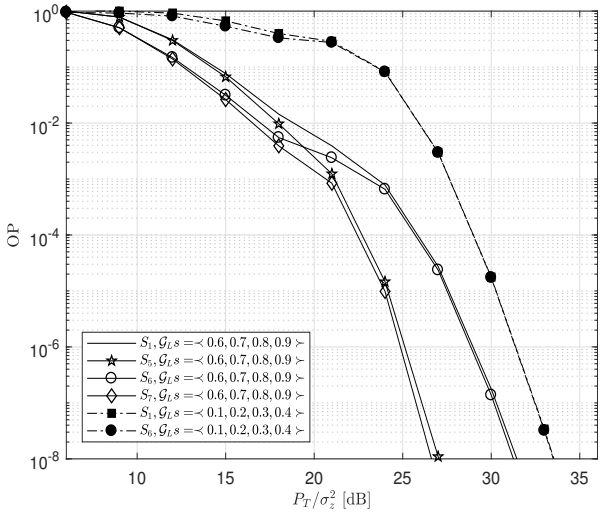

Fig. 4. OP for various cases with $M = 4$ and $K = 3$.

- The OPs are bounded by two extreme cases: i) a LoS-rich environment; and ii) a nLoS-rich environment.
- Since the nLoS path has a greater path-loss exponent than the LoS path, a lower OP is obtained as $\mathcal{G}_{\rm L}$ increases.
- Except the LoS-rich environment, as the SNR increases, the asymptotic OP is tend to be determined by the OP related with the nLoS path since $\sum_{m=1}^{5} N_{m,\rm L} > \sum_{m=1}^{5} N_{m,\rm nL}$. See proof of Corollary 6.
- When $\mathcal{G}_{\rm L} s =\prec 0.0, 0.4, 0.4, 0.4, 0.4 \succ$, the first nLoS path makes the OP approach rapidly to that of the nLoS-rich environment comparing with the case of $\mathcal{G}_{\rm L} s =\prec 0.4, 0.4, 0.4, 0.4, 0.4 \succ$. See proof of Corollary 6.
- A single nLoS path has a much greater effect on the OP when other paths have a lower selection probability of LoS path. For example, $\mathcal{G}_{\rm L} s =\prec 0.0, 0.4, 0.4, 0.4, 0.4 \succ$ vs. $\mathcal{G}_{\rm L} s =\prec 0.0, 0.8, 0.8, 0.8, 0.8 \succ$.
- Comparing with the case of $K = 1$, which corresponds to the system of [32] and [33], dCDD enables effective RRU cooperation, so that dCDD with $K = 3$ can realize an OP of $1e^{-8}$ with a 3.8 dB SNR gain. However, in the high SNR region, the slope, i.e., the diversity gain, is similarly independent of K. Thus, this can be an additional proof for Corollary 6.

3) Impact of the number of multipath components on the OP: In Fig. 4, we investigate impact of the number of multipath components on the OP, which is obtained via (21), under two different set of $\mathcal{G}_{\rm L}$s, i.e., $\prec 0.6, 0.7, 0.8, 0.9 \succ$ and $\prec 0.1, 0.2, 0.3, 0.4 \succ$. For $M = 4$ and $K = 3$, We can observe the following facts

- When dCDD is running in the environment where the nLoS path appears more frequently, the OP differences due to different number of multipath components over the LoS path is negligible as the SNR increases. For example, scenario $\mathbb{S}_1$ vs. scenario $\mathbb{S}_6$ with $\mathcal{G}_{\rm L} s =\prec 0.1, 0.2, 0.3, 0.4 \succ$.
- In general, when the LoS path appears more frequently in the target environment, the number of multipath components of the LoS path impacts the OP up to the middle SNR regions. For example, scenario $\mathbb{S}_5$ vs. scenario $\mathbb{S}_6$ with $\mathcal{G}_{\rm L} s =\prec 0.6, 0.7, 0.8, 0.9 \succ$. However, as the SNR increases, the asymptotic OP is determined by the number of multipath components of the nLoS path. Furthermore, for $\mathcal{G}_{\rm L} s =\prec 0.6, 0.7, 0.8, 0.9 \succ$, $\mathbb{S}_7$ results in a lower OP comparing with $\mathbb{S}_6$ since $\min(\sum_{m=1}^{4} N_{m,\rm L}, \sum_{m=1}^{4} N_{m,\rm nL})$ is greater for $\mathbb{S}_7$.

4) Impact of the distance on the OP: For this scenario, we assume that the location of the RX is on a line through two ending points $(3 - j3)$ and $(11 + j3)$. Based on the approach proposed by [49], $\mathcal{G}_{m,\rm L}$ is determined by the following probability model

$$\mathcal{G}_{m,\rm L} = \min(D_1/d_m, 1)(1 - e^{-d_m/D_2}) + e^{-d_m/D_2} \quad (33)$$

for d_m, a distance from the mth RRU to the RX. In (33), $D_1 = 1.854$ and $D_2 = 39.71$ are determined by the distribution of all the distances measured from the considered system setup. D_1 is set to a distance in which 10% of all distances should lie, whereas D_2 is set to four times of a distance in which 99% of all distances should lie. For the first four RRUs, (33) provides $\mathcal{G}_{\rm L} s =\prec 0.8962, 0.94445, 0.9761, 0.96267 \succ$, $\mathcal{G}_{\rm L} s =\prec 0.9294, 0.9565, 0.9474, 0.9101 \succ$, $\mathcal{G}_{\rm L} s =\prec 0.8584, 0.9076, 0.9511, 0.9695 \succ$, and $\mathcal{G}_{\rm L} s =\prec 0.8927, 0.95052, 1.0, 1.0 \succ$, for the RX respectively located at $(4-j2.25)$,$(6-j0.75)$,$(8+j0.75)$, and $(10+j2.25)$.

For the different locations of the RX, Fig. 5 shows the OP of the case with $M = 4$, $K = 3$, and scenario $\mathbb{S}_1$. Since a large-scale fading depends on the distance from the RRU to RX, the location of the RX also influences the OP. As the RX is close to the ending location, $(11+j3)$, the distances from the RRUs are decreased and it enters the LoS-rich environment. Thus, at the same small-scale fading severity, a lower OP is obtained. Comparing with the system without dCDD, i.e., $K = 1$, RRU

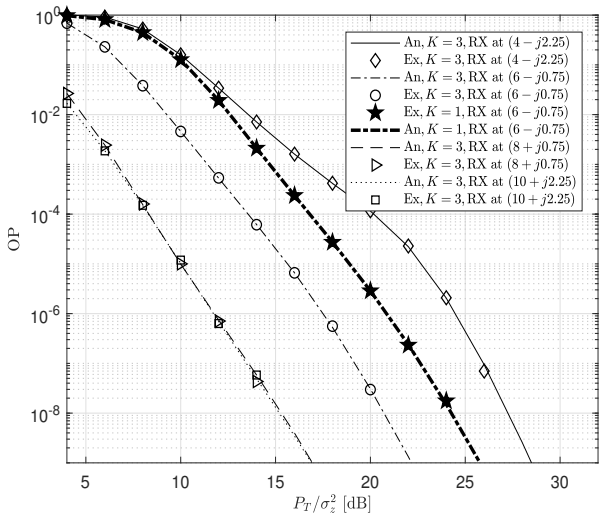

Fig. 5. OP for various locations of the RX.

cooperation by dCDD attributes a lower OP. However, we can observe that the slope will be similar in the high SNR region even for $K = 1$.

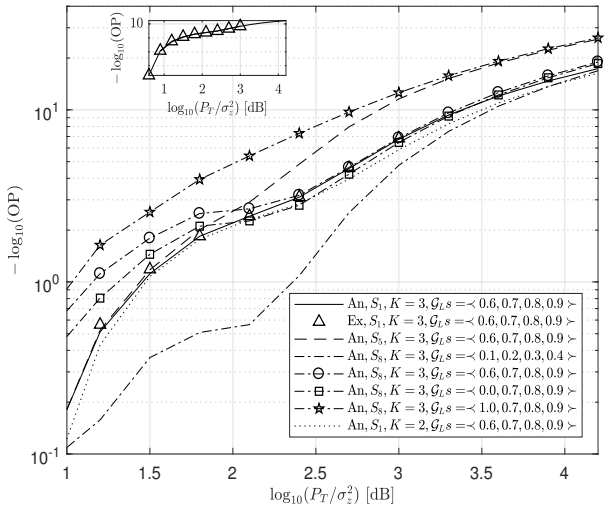

Fig. 6. OP for various cases in the $\log_{10} - \log_{10}$ scale. Analytically derived expressions are used for the OP.

5) Asymptotic OP analysis: We now conduct the diversity gain analysis of the CP-SC system based on the asymptotic OP. For various scenarios, we compute the diversity gain, G_d, derived from *Theorem 2*, which verifies that $G_d = \sum_{m=1}^{M} \min(N_{m,\mathrm{L}}, N_{m,\mathrm{nL}})$. By measuring the slope of the outage probability provided in Fig. 6, we can compute the diversity gain in the high SNR regions as follows. We use a fixed $M = 4$.

- Scenario $\mathbb{S}_1$ with a different value of K. For example, dCDD with two RRUs results in the same diversity gain as that of three dCDD RRUs. Its slopes are measured as 8.88 and 8.92 respectively for $K = 3$ and $K = 2$. The exact diversity gain is $G_d = 10$. Thus, K does not determine the diversity gain, which is proved by Corollary 6.
- In contrast to scenario $\mathbb{S}_1$, scenario $\mathbb{S}_5$ results in a lower outage probability due to nLoS paths. However, scenario $\mathbb{S}_5$ results in the same slope due to LoS paths that determine the slope. A measured slope is given by 9.7, whereas the exact diversity gain is $G_d = 10$.
- For scenario $\mathbb{S}_8$, we investigate the impact of $\mathcal{G}_\mathrm{L}$s on the asymptotic diversity gain. For different values of $\mathcal{G}_\mathrm{L}$s, a same slope, 10.1, is measured comparing with the exact diversity gain, $G_d = 11$. This is valid even if one path is in the nLoS-rich environment. Especially, when one path is in the LoS-rich environment, it results in a 10 dB improvement in achieving an $1e^{-10}$ OP, without changing the diversity gain.

B. Performance analysis in terms of SE

An analytically derived SE is obtained via (23).

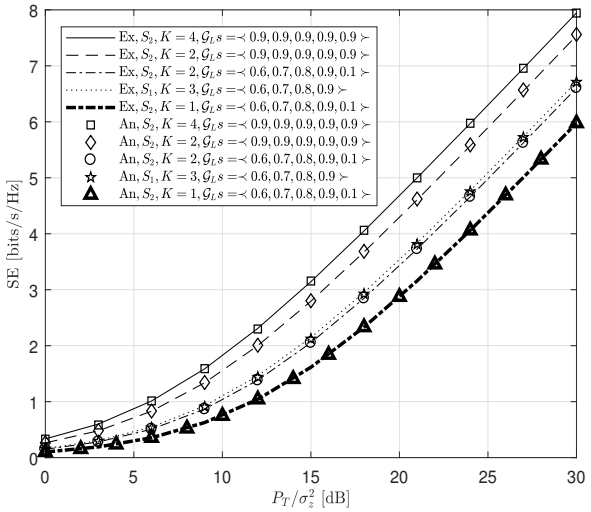

Fig. 7. SE for various scenarios.

1) Accuracy of the derivation: We first investigate the spectral efficiency for various scenarios. The results are provided in Fig. 7. This figure shows that for all the considered scenarios, the developed closed-expression for the SE provides very accurate results comparing with those of link-level simulations. This figure also shows that for scenario $\mathbb{S}_2$ and $\mathcal{G}_\mathrm{L} s =\prec 0.6, 0.7, 0.8, 0.9, 0.1 \succ$, greater RRU cooperation by dCDD, i.e., $K = 2$, results in about a 0.5 bits/s/Hz increased SE at 20 dB SNR comparing with the case of $K = 1$, which corresponds to the system of [32] and [33].

2) Impact of selection probability of LoS path on the SE: Since the selection probability of LoS path is one of the key parameters in determining the performance, we investigate its impact on the SE. In generating Fig. 8, we assume $M = 5$, the same $\mathcal{G}_\mathrm{L} \triangleq \mathcal{G}_{m,\mathrm{L}}$ for all the paths, and a fixed SNR, $\frac{P_T}{\sigma_z^2} = 24$ dB. Thus, we mainly investigate the impact of the selection probability of LoS path on the SE for a different number of the

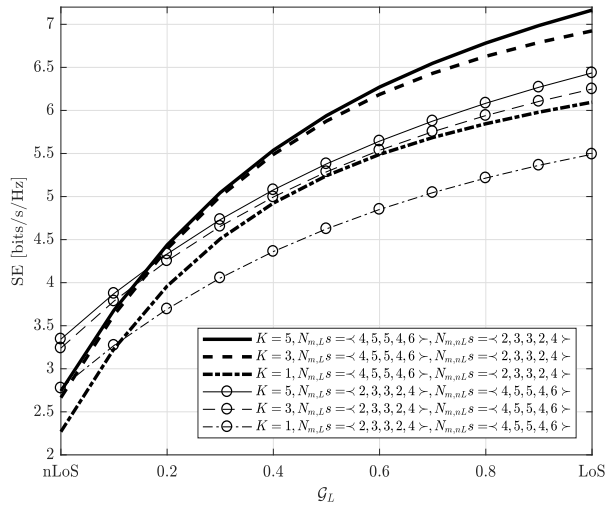

Fig. 8. SE for various values of $\mathcal{G}_L$s.

dCDD RRUs. For two scenarios: (1) the number of multipath components of LoS paths is greater than that of nLoS paths; and (2) the number of multipath components of LoS paths is less than that of nLoS paths. From the both scenarios, we can observe the following facts:

- A greater SE is achieved as $\mathcal{G}_{\mathrm{L}}$ increases since LoS paths become dominant.
- When the number of multipath components of LoS paths is greater than that of nLoS paths, the rate of change of the SE with respect to $\mathcal{G}_{\mathrm{L}}$ is greater than other scenario.
- For the considered channel environments, the performance gap for with $K = 5$, $K = 3$, and $K = 1$ increases as $\mathcal{G}_{\mathrm{L}}$ increases. This gap is particularly noticeable as K is increased.

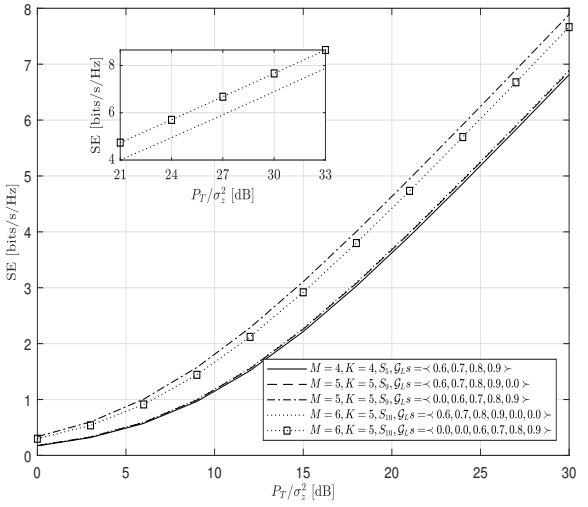

Fig. 9. SE for various values of M, K, and the number of multipath components.

3) Impact of the number of multipath components on the SE: In Fig. 9, we investigate the impact from various parameters on the SE. We can make the following observations.

- As M increases, a greater SE is achieved due to an increased diversity gain. For example, $M = 4, K = 4$ vs. $M = 5, K = 5$ and $M = 6, K = 5$.
- Even if the additional paths are only for nLoS, a greater SE can be achieved. For example, $M = 4, K = 4$ vs. $M = 5, K = 5$ with $\mathcal{G}_{\mathrm{L}}s =\prec 0.6, 0.7, 0.8, 0.9, 0.0 \succ$ and $\mathcal{G}_{\mathrm{L}}s =\prec 0.0, 0.6, 0.7, 0.8, 0.9 \succ$. An increased diversity gain causes this result.
- When the additional paths are only for nLoS, the number of numtipath components over the nLoS path determines the SE. For example, $M = 5, K = 5$ with $\mathcal{G}_{\mathrm{L}}s =\prec 0.6, 0.7, 0.8, 0.9, 0.0 \succ$ and $\mathcal{G}_{\mathrm{L}}s =\prec 0.0, 0.6, 0.7, 0.8, 0.9 \succ$. Since $N_{1,\mathrm{nL}} = 5$ and $N_{5,\mathrm{nL}} = 1$, $\mathcal{G}_{\mathrm{L}}s =\prec 0.0, 0.6, 0.7, 0.8, 0.9 \succ$ results in a greater SE among two considered scenarios. A similar observation can be made for $M = 6, K = 5$ with two additional nLoS paths.
- *Corollary 6* and *Corollary 7* are related with the above observations.

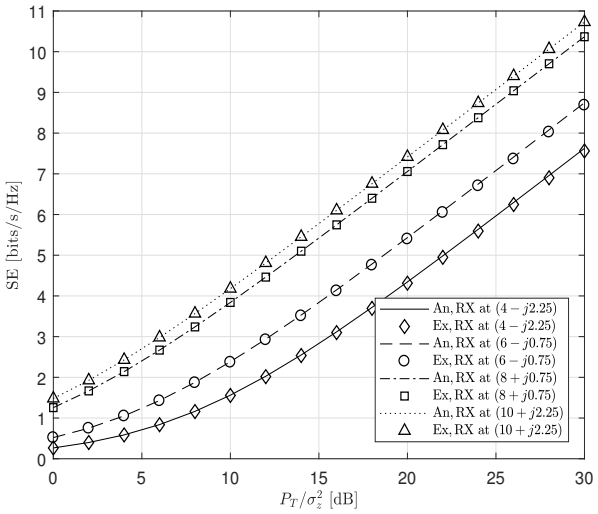

Fig. 10. SE for various locations of the RX.

4) Impact of the distance on the SE: For the same simulation setting for Fig.5, Fig.10 shows the impact of the distance on the SE. As the RX is close to the ending location, $(11+j3)$, the distances are decreased. Thus, signal-power attenuation is decreased, which makes the considered system achieve a greater SE.

V. Conclusions

In this paper, we have derived the diversity gain of dCDD being used in distributed CP-SC system, which is overpopulated with RRHs, in non-identical frequency selective fading channels, which coexist with LoS and nLoS paths. For these channels, generalized closed-form expressions for the distributions of the SNR realized at the receiver have been derived.

To achieve reliable and accurate performance measurement metrics, several approaches, such as order statistics, spacing statistics, and approximation of the summation of gamma distributions, have been jointly applied. For various simulation scenarios, it has been seen that the selection probability of the LoS path, number of the RRUs for dCDD, number of multipath components are key parameters that determine the outage probability. According to the asymptotic analysis in the high SNR region, the maximum diversity gain has been derived and justified by the link level simulations. Similar performance behavior of the spectral efficiency has been verified for various simulation scenarios. Even for a particular LoS path selection probability model, the proposed derivations have been shown to provide an accurate outage probability and spectral efficiency. By converting the multiple-input and single-output frequency selective fading channels into a highly frequency selective fading channel, and applying effective signal processing at the RRUs that leads to ISI-free reception at the receiver, dCDD enables the distributed CP-SC system to achieve the maximum diversity gain.

Appendix A: Derivation of Theorem 1

We first rewrite $\mathrm{Per}\boldsymbol{A}_K$ as follows:

$$\mathrm{Per}\boldsymbol{A}_K = \sum_{\substack{n_1,\ldots,n_K \\ n_1\neq n_2\neq\ldots\neq n_K}} \mathbb{C}_{M,K} e^{-x_1(\breve{a}_1+\sum_{i=K+1}^{M}\tilde{a}_i)} (x_1)^{\breve{m}_1+\sum_{i=K+1}^{M}\tilde{m}_i-1} \prod_{i=2}^{K} e^{-\breve{a}_i x_i}(x_i)^{\breve{m}_i-1} \quad \text{(A.1)}$$

where $\mathbb{C}_{M,K} \triangleq \big(\prod_{i=1}^{K}\mathbb{Y}_{n_i}\prod_{i=K+1}^{M}\mathbb{X}_i\big)$, $\breve{a}_i \triangleq \breve{a}_{n_i}$, $\breve{m}_i \triangleq \breve{m}_{n_i}$, and $\tilde{a}_{n_i} \triangleq \tilde{a}_i$. Thus, the MGF of γ is given by

$$M_\gamma(s) = \int_0^\infty \int_{x_1}^\infty \ldots \int_{x_{M-2}}^\infty \int_{x_{M-1}}^\infty e^{-s(\sum_{j=1}^{K} x_j)} \mathrm{Per}\tilde{\boldsymbol{A}}_K \, dx_M \ldots dx_2 dx_1. \quad \text{(A.2)}$$

In general, the computation of (A.2) is possible only for $K=1$ and $K=2$ since X_is are order statistics, which are dependent on one another. Thus, we apply the spacing statistics $Y_i = X_i - X_{i-1}$ with $X_1 = Y_1$, i.e., $X_i = \sum_{j=1}^{i} Y_i$. Having applied the spacing statistics, (A.2) can be evaluated as

$$M_\gamma(s) = \int_0^\infty \int_0^\infty \ldots \int_0^\infty \int_0^\infty e^{-s(\sum_{j=1}^{K}\sum_{i=1}^{j} y_i)} \mathrm{Per}\boldsymbol{A}_K \, dy_M \ldots dy_2 dy_1. \quad \text{(A.3)}$$

where $\mathrm{Per}\boldsymbol{A}_K$ is also converted into the following form

$$\mathrm{Per}\boldsymbol{A}_K = \widetilde{\sum_{\substack{n_1,\ldots,n_K \\ n_1\neq n_2\neq\ldots\neq n_K}}} e^{-y_1(\sum_{j=1}^{K}\breve{a}_j+\sum_{i=K+1}^{M}\tilde{a}_i)} y_1^{(\breve{m}_1+\sum_{j=2}^{K}\boldsymbol{a}_{j,|j|}(1)+\sum_{i=K+1}^{M}\tilde{m}_i-1)} e^{-y_2(\sum_{j=2}^{K}\breve{a}_j)} y_2^{(\sum_{j=2}^{K}\boldsymbol{a}_{j,|j|}(2))} e^{-y_3(\sum_{j=3}^{K}\breve{a}_j)} y_3^{(\sum_{j=3}^{K}\boldsymbol{a}_{j,|j|}(3))} \ldots e^{-y_K(\sum_{j=K}^{K}\breve{a}_j)} y_K^{(\sum_{j=K}^{K}\boldsymbol{a}_{j,|j|}(K))} \quad \text{(A.4)}$$

where $\widetilde{\sum}_{\substack{n_1,\ldots,n_K \\ n_1\neq n_2\neq\ldots\neq n_K}} \triangleq \sum_{\substack{n_1,\ldots,n_K \\ n_1\neq n_2\neq\ldots\neq n_K}} \mathbb{C}_{M,K} \sum_{\mathrm{sum}(\boldsymbol{a}_{2,|2|})=\breve{m}_2-1} \binom{\breve{m}_2-1}{\boldsymbol{a}_{2,|2|}} \ldots \sum_{\mathrm{sum}(\boldsymbol{a}_{K,|K|})=\breve{m}_K-1} \binom{\breve{m}_K-1}{\boldsymbol{a}_{K,|K|}}$ with $\boldsymbol{a}_{2,|2|} \in \mathbb{N}_0^{|2|}, \ldots, \boldsymbol{a}_{K,|K|} \in \mathbb{N}_0^{|2|}$. Note that the multinomial theorem is used in the derivation of (A.4) as $(\sum_{j=1}^{i} y_j)^{\breve{m}_i-1} = \sum_{\mathrm{sum}(\boldsymbol{a}_{i,|i|})=\breve{m}_i-1} \binom{\breve{m}_i-1}{\boldsymbol{a}_{i,|i|}} \prod_{j=1}^{i}(y_j)^{\boldsymbol{a}_{i,|i|}(j)}$. Note that except the term related to y_1, others have a similar form. Since y_js are independent of one another, and the domain of y_is is all positive values, i.e., $0 \le y_j \le \infty$, the spacing statistics makes us to derive the final expression for the MGF of γ as shown in (17).

Appendix B: Derivation of *Corollary 3*

According to [45], we first express $\prod_{m=1}^{K}(s+q_m)^{-e_m}$ as follows:

$$\prod_{m=1}^{K}(s+q_m)^{-e_m} = (b_I)^{F_d}(1+b_I s)^{-F_d}\big(1-\frac{x_1}{1+b_I s}\big)^{-e_1} \ldots \big(1-\frac{x_M}{1+b_I s}\big)^{-e_M} \quad \text{(B.1)}$$

where $b_I = \min(1/q_1, \ldots, 1/q_M)$ and $x_i \triangleq 1 - b_I q_i$. When $\big|\frac{x_i}{1+b_I S}\big| < 1$, (B.1) can be further expressed alternatively as follows:

$$\prod_{m=1}^{K}(s+q_m)^{-e_m} = (b_I)^{F_d}(1+b_I s)^{-F_d} e^{(\sum_{l=0}^{\infty} r_l (1+b_I s)^{-l})} \quad \text{(B.2)}$$

where $r_l = \sum_{m=1}^{K} \frac{e_m}{l}(1-b_I q_m)^l$. By evaluating $e^{(\sum_{l=0}^{\infty} r_l(1+b_I s)^{-l})} = 1 + \delta_1(1-b_I q_m)^{-1} + \delta_2(1-b_I q_m)^{-2} + \ldots$, and taking the derivative of both sides, a recursive form for δ_k can be derived as $\delta_{k+1} = (r_1\delta_k + \ldots + (k+1)r_{k+1}\delta_0)/(k+1)$ with $\delta_0 = 1$. Thus, we can derive

$$\prod_{m=1}^{K}(s+q_m)^{-e_m} = \sum_{l=0}^{\infty} \delta_l (b_I)^{-l}(1/b_I + s)^{-G_d-l}. \quad \text{(B.3)}$$

References

[1] K. J. Kim, M. D. Renzo, H. Liu, P. V. Orlik, and H. V. Poor, "Diversity gain analysis of distributed CDD systems in non-identical frequency selective fading," in *Proc. IEEE Int. Conf. Commun.*, Kansas City, MO, May 2018, pp. 1 – 6.

[2] J. Mietzner, "A survey of resource management toward 5G radio access networks," *IEEE Commun. Surveys Tuts.*, vol. 18, no. 3, pp. 1656–1686, 2016.

[3] M. Agiwal, A. Roy, and N. Saxena, "Next generation 5G wireless networks: A comprehensive survey," *IEEE Commun. Surveys Tuts.*, vol. 18, no. 3, pp. 1617–1655, 2016.

[4] A. Gupta and R. K. Jha, "A survey of 5G network: Architecture and emerging technologies," *IEEE Access*, vol. 3, pp. 1206–1232, 2015.

[5] G. Fettweis and S. Alamouti, "5G: Personal mobile internet beyond what cellular did to telephony," *IEEE Commun. Mag.*, vol. 52, no. 2, pp. 140–145, 2014.

[6] B. Bangerter, S. Talwar, R. Arefi, and K. Stewart, "Networks and devices for the 5G era," *IEEE Commun. Mag.*, vol. 52, no. 2, pp. 90–96, 2014.

[7] B. Hochwald, T. L. Marzetta, and C. B. Papadias, "A transmitter diversity scheme for wideband CDMA systems based on space-time spreading," *IEEE J. Sel. Areas Commun.*, vol. 19, no. 1, pp. 48–60, Jan. 2001.

[8] S. M. Alamouti, "A simple transmit diversity technique for wireless communications," *IEEE J. Sel. Areas Commun.*, vol. 16, no. 8, pp. 1451–1458, Oct. 1998.

[9] J. N. Laneman and G. W. Wornell, "Energy-efficient antenna sharing and relaying for wireless networks," in *Proc. IEEE Wireless Commun. and Netw. Conf.*, Chicago, IL, May 2000, pp. 7–12.

[10] M. O. Astal and A. M. Abu-Hudrouss, "SIC detector for 4 relay distributed space-time block coding under quasi-synchronization," *IEEE Commun. Lett.*, vol. 15, no. 10, pp. 1056–1058, Oct. 2011.

[11] M. M. Aldosari and K. A. Hamdi, "Energy efficiency of distributed antenna systems using fractional frequency reuse," *IEEE Commun. Lett.*, vol. 19, no. 11, pp. 1985–1988, Nov. 2015.

[12] K. J. Kim, T. Khan, and P. Orlik, "Performance analysis of cooperative systems with unreliable backhauls and selection combining," *IEEE Trans. Veh. Technol.*, vol. 66, no. 3, pp. 2448–2461, Mar. 2017.

[13] J. N. Laneman, D. N. C. Tse, and G. W. Wornell, "Cooperative diversity in wireless networks: Efficient protocols and outage behavior," *IEEE Trans. Inf. Theory*, vol. 50, no. 12, pp. 3062–3080, Dec. 2004.

[14] J. K. Cavers, "Single-user and multiuser adaptive maximal ratio transmission for Rayleigh channels," *IEEE Trans. Veh. Technol.*, vol. 49, no. 6, pp. 2043–2050, Nov. 2000.

[15] T. K. Y. Lo, "Maximum ratio transmission," *IEEE Trans. Commun.*, vol. 47, no. 10, pp. 1458–1461, Oct. 1999.

[16] IEEE P802.11ac, "Wireless LAN medium access control (MAC) and physical layer (PHY) specifications–Amendment 4: Enhancements for very high throughput for operation in bands below 6 GHz," 2009.

[17] IEEE P802.11n/D1.04, "Wireless LAN medium access control (MAC) and physical layer (PHY) specifications - Amendment 5: Enhancements for higher throughput," 2009.

[18] 3GPP, R1-061192, "Channel dependent scheduling with cyclic delay diversity," May 2006.

[19] A. H. Mehana and A. Nosratinia, "Single-carrier frequency-domain equalizer with multi-antenna transmit diversity," *IEEE Trans. Wireless Commun.*, vol. 12, pp. 388–397, Jan. 2013.

[20] Y.-C. Liang, W. S. Leon, Y. Zeng, and C. Xu, "Design of cyclic delay diversity for single carrier cyclic prefix (SCCP) transmissions with block-iterative GDFE (BI-GDFE) receiver," *IEEE Trans. Wireless Commun.*, vol. 7, no. 2, pp. 677–684, Feb. 2008.

[21] U.-K. Kwon and G.-H. Im, "Cyclic delay diversity with frequency domain Turbo equalization for uplink fast fading channels," *IEEE Commun. Lett.*, vol. 13, no. 3, pp. 184–186, Mar. 2009.

[22] Q. Li, Q. Yan, K. C. Keh, K. H. Li, and Y. Hu, "A multi-relay-selection scheme with cyclic delay diversity," *IEEE Commun. Lett.*, vol. 17, no. 2, pp. 349–352, Feb. 2013.

[23] G. Wu, Q. Du, and K. Hua, "Selective random CDD enhanced joint cooperative relay and HARQ for delay-tolerant vehicular communications," *International Journal of Distributed Sensor Networks*, vol. 11, no. 5, May 2015.

[24] IEEE P802.11ad/D0.1, "Wireless LAN medium access control (MAC) and physical layer (PHY) specications: enhancements for very high throughput in the 60GHz band," *IEEE P802.11ad/D0.1*, Jun. 2010.

[25] S. Kato, H. Harada, R. Funada, T. Baykas, C. S. Sum, J. Wang, and M. A. Rahman, "Single carrier transmission for multi-gigabit 60-GHz WPAN systems," *IEEE J. Sel. Areas Commun.*, vol. 27, no. 8, pp. 1466–1478, Oct. 2009.

[26] K. J. Kim, M. D. Renzo, H. Liu, P. V. Orlik, and H. V. Poor, "Performance analysis of distributed single carrier systems with distributed cyclic delay diversity," *IEEE Trans. Commun.*, vol. 65, no. 12, pp. 5514–5528, Dec. 2017.

[27] K. J. Kim, H. Liu, M. Wen, M. D. Renzo, and H. V. Poor, "Outage probability analysis of spectrum sharing systems with distributed cyclic delay diversity," *IEEE Trans. Commun.*, vol. 67, no. 6, pp. 4435–4449, Jun. 2019.

[28] N. Iradukunda, H. T. Nguyen, and W. Hwang, "On cyclic delay diversity-based single-carrier scheme in spectrum sharing systems," *IEEE Commun. Lett.*, vol. 23, no. 6, pp. 1069–1072, Jun. 2019.

[29] K. J. Kim, H. Liu, M. D. Renzo, P. V. Orlik, and H. V. Poor, "Secrecy analysis of distributed CDD-based cooperative systems with deliberate interference," *IEEE Trans. Wireless Commun.*, vol. 17, no. 12, pp. 7865–7878, Dec. 2018.

[30] K. J. Kim, H. Liu, M. Wen, P. Orlik, and H. V. Poor, "Secrecy performance analysis of distributed asynchronous cyclic delay diversity-based cooperative single carrier systems," *IEEE Trans. Commun.*, vol. 68, no. 5, pp. 2680–2694, May 2020.

[31] K. J. Kim, M. D. Renzo, H. Liu, T. A. Tsiftsis, P. V. Orlik, and H. V. Poor, "Distributed cyclic delay diversity systems with spatially distributed interferers," *IEEE Trans. Wireless Commun.*, vol. 18, no. 4, pp. 2066 –2079, Apr. 2019.

[32] K. J. Kim, T. A. Tsiftsis, and H. V. Poor, "Power allocation in cyclic prefixed single-carrier relaying systems," *IEEE Trans. Wireless Commun.*, vol. 10, no. 7, pp. 2297–2305, Jul. 2011.

[33] K. J. Kim and T. A. Tsiftsis, "On the performance of cyclic prefix-based single-carrier cooperative diversity systems with best relay selection," *IEEE Trans. Wireless Commun.*, vol. 10, no. 4, pp. 1269–1279, Apr. 2011.

[34] K. Alam and K. T. Wallenius, "Distribution of a sum of order statistics," *Scandinavian Journal of Statistics*, vol. 6, no. 3, pp. 845–855, 1979.

[35] S. S. Nam, M. O. Hasna, and M. Alouini, "Joint statistics of partial sums of ordered exponential variates and performance of GSC RAKE receivers over Rayleigh fading channels," *IEEE Trans. Commun.*, vol. 59, no. 8, pp. 2241–2253, Aug. 2011.

[36] E. Bedeer and M. J. Hossain, "Performance of low-complexity uniform power loading OFDM systems with reduced feedback over rayleigh fading channels," *IEEE Trans. Wireless Commun.*, vol. 15, no. 6, pp. 3783–3795, Jun. 2016.

[37] N. Balakrishnan, "Permanents, order statistics, outliers, and robustness," *Rev. Mat. Complu.*, vol. 20, pp. 7–107, 2007.

[38] H. A. David and H. N. Nagaraja, *Order Statistics*, 3rd ed. Hoboken, New Jersey: John Wiley and Sons, 2005.

[39] K. J. Kim, S. Y. Kwon, E. K. Hong, and K. C. Whang, "Comments on Comparison of diversity combining techniques for Rayleigh-fading channels," *IEEE Trans. Commun.*, vol. 46, no. 9, pp. 1109–1110, Sep. 1999.

[40] IEEE Std 1588-2008, "A precision clock synchronization protocol for networked measurement and control systems," *IEEE Standard 1588-2008*, Jul. 2008.

[41] A. Mahmood, R. Exel, H. Trsek, and T. Sauter, "Clock synchronization over IEEE 802.11–A survey of methodologies and protocols," *IEEE Trans. Ind. Informat.*, vol. 13, no. 2, pp. 907–922, Apr. 2017.

[42] H. Zhang, Y. Dong, J. Cheng, M. J. Hossain, and V. C. M. Leung, "Fronthauling for 5G LTE-U ultra dense cloud small cell networks," *IEEE Wireless Communications*, vol. 23, no. 6, pp. 48–53, Dec. 2016.

[43] 3GPP, TS 36.211 (V8.9.0), "Evolved universal terrestrial radio access (E-UTRA): Physical channels and modulation," Mar. 2009.

[44] I. S. Gradshteyn and I. M. Ryzhik, *Table of Integrals, Series, and Products*. New York: Academic Press, 2007.

[45] P. G. Moschopoulos, "The distribution of the sum of independent gamma random variables," *Ann. Inst. Statist. Math. (PartA)*, vol. 37, pp. 541–544, 1985.

[46] V. S. Adamchik and O. I. Marichev, "The algorithm for calculating integrals of hypergeometric type functions and its realization in REDUCE system," in *Proc. Int. Conf. Symbolic Algebraic Computation*, Tokyo, Japan, Aug. 1990, pp. 3829–3833.

[47] Wolfram Research Inc. The Mathematical Functions Site. Accessed: Oct.13, 2019. [Online]. Available: http://functions.wolfram.com

[48] 3GPP, TR 36.828 (V11.0.0), "Further enhancements to LTE time division duplex (TDD) for downlink-uplink (DL-UL) interference management and traffic adaptation," Jun. 2012.

[49] 3GPP, TR 36.873 (V12.2.0), "Study on 3D channel model for LTE," Jul. 2015.